Tectonophysics 663 (2015) 261–274

Contents lists available at ScienceDirect

Tectonophysics

journal homepage: www.elsevier.com/locate/tecto

Moment tensor solutions for the Iberian-Maghreb region during the IberArray deployment (2009–2013)

R. Martín [a,*], D. Stich [a,b], J. Morales [a,b], F. Mancilla [a,b]

[a] Instituto Andaluz de Geofisica, Universidad de Granada, Granada, Spain
[b] Departamento de Fisica Teórica y del Cosmos, Universidad de Granada, Granada Spain

ARTICLE INFO

Article history:
Received 31 January 2015
Received in revised form 27 June 2015
Accepted 11 August 2015
Available online 29 August 2015

Keywords:
IberArray
Moment tensor inversion
Seismotectonics
Iberia-Maghreb region

ABSTRACT

We perform regional moment tensor inversion for 84 earthquakes that occurred in the Iberian-Maghreb region during the second and third leg of IberArray deployment (2009–2013). During this period around 300 seismic broadband stations were operating in the area, reducing the interstation spacing to ~50 km over extended areas. We use the established processing sequence of the IAG moment tensor catalogue, increasing to 309 solutions with this update. New moment tensor solutions present magnitudes ranging from Mw 3.2 to 6.3 and source depths from 2 to 620 km. Most solutions correspond to Northern Algeria, where a compressive deformation pattern is consolidated. The Betic-Rif sector shows a progression of faulting styles from mainly shear faulting in the east via predominantly extension in the central sector to reverse and strike-slip faulting in the west. At the SW Iberia margin, the predominance of strike-slip and reverse faulting agrees with the expected transpressive character of the Eurasian-Nubia plate boundary. New strike-slip and oblique reverse solutions in the Trans-Alboran Shear Zone reflect its left-lateral regime. The most significant improvement corresponds to the Atlas Mountains and the surroundings of the Gibraltar Arc with scarce previous solutions. Reverse and strike-slip faulting solutions in the Atlas System display the accommodation of plate convergence by shortening in the belt. At the Gibraltar Arc, several new solutions were obtained at lower crustal and subcrustal depths. These mechanisms show substantial heterogeneity, covering the full range of faulting styles with highly variable orientations of principal stress axes, including opposite strike slip faulting solutions at short distance. The observations are not straightforward to explain by a simple geodynamic scenario and suggest the interplay of different processes, among them plate convergence in old oceanic lithospheric with large brittle thickness at the SW Iberia margin, as well as delamination of thickened continental lithosphere beneath the Betic-Rif arc.

1. Introduction

The Iberian-Maghreb region, including the Iberian Peninsula, North Africa and nearby offshore areas in the Mediterranean Sea and Atlantic Ocean, is situated at the Eurasia-Africa plate boundary (Fig. 1a). However, seismicity in this region is only partly controlled by the NW–SE to WNW–ESE Nubia-Eurasian plate convergence motion of ~5 mm/yr (DeMets et al., 1994; Calais et al., 2003; McClusky et al., 2003; Serpelloni et al., 2007), and the geographical distribution of earthquakes, their focal mechanism and source depths show complex patterns across the region. The main concentration of seismicity occurs along a wide zone from the Gorringe Bank in the Atlantic Ocean into southern Spain and to the Tell Atlas in North Algeria, as well as along an orthogonal fault zone from Southeastern Iberia to North Morocco crossing the Alboran Sea (The Trans-Alboran shear zone-TASZ) (Buforn et al., 1995, 2004; Stich et al., 2003, 2006, 2010). The hypocenters show a relatively wide distribution and do not delineate a linear Africa-Eurasian plate boundary clearly. Intraplate seismicity accompanies deformation on either side of the plate boundary zone, in the interior and north of the Iberian Peninsula as well as in the interior of the Maghrebian margin. Secondary concentrations of seismicity can be observed near deformed mountain belts far off the presumed plate contact, like the Pyrenees and the Atlas System (Fig. 1b). Most earthquakes over the region show shallow source depths (0–40 km), however subcrustal earthquakes are documented around the Alboran Sea (Buforn et al., 2004) as well as at the Southwest Iberian Atlantic margin (Stich et al., 2005a), with this latter being a source of large and tsunamigenic earthquakes such as the 1755 Lisbon earthquake and tsunami (e.g., Bartolomé et al., 2009; Martínez Solares and López Arroyo, 2004; Stich et al., 2007). The faulting style over the Iberian-Maghreb region ranges from pure reverse to pure normal focal mechanisms (e.g., Stich et al., 2003), showing a pronounced geographical variability as well as local heterogeneity of faulting in several areas (e.g., Stich et al., 2010).

* Corresponding author at: Instituto Andaluz de Geofísica Campus Universitario de Cartuja C/ Profesor Clavera, 12 . 18071, Granada (Spain)
E-mail address: rosa@ugr.es (R. Martín).

http://dx.doi.org/10.1016/j.tecto.2015.08.012

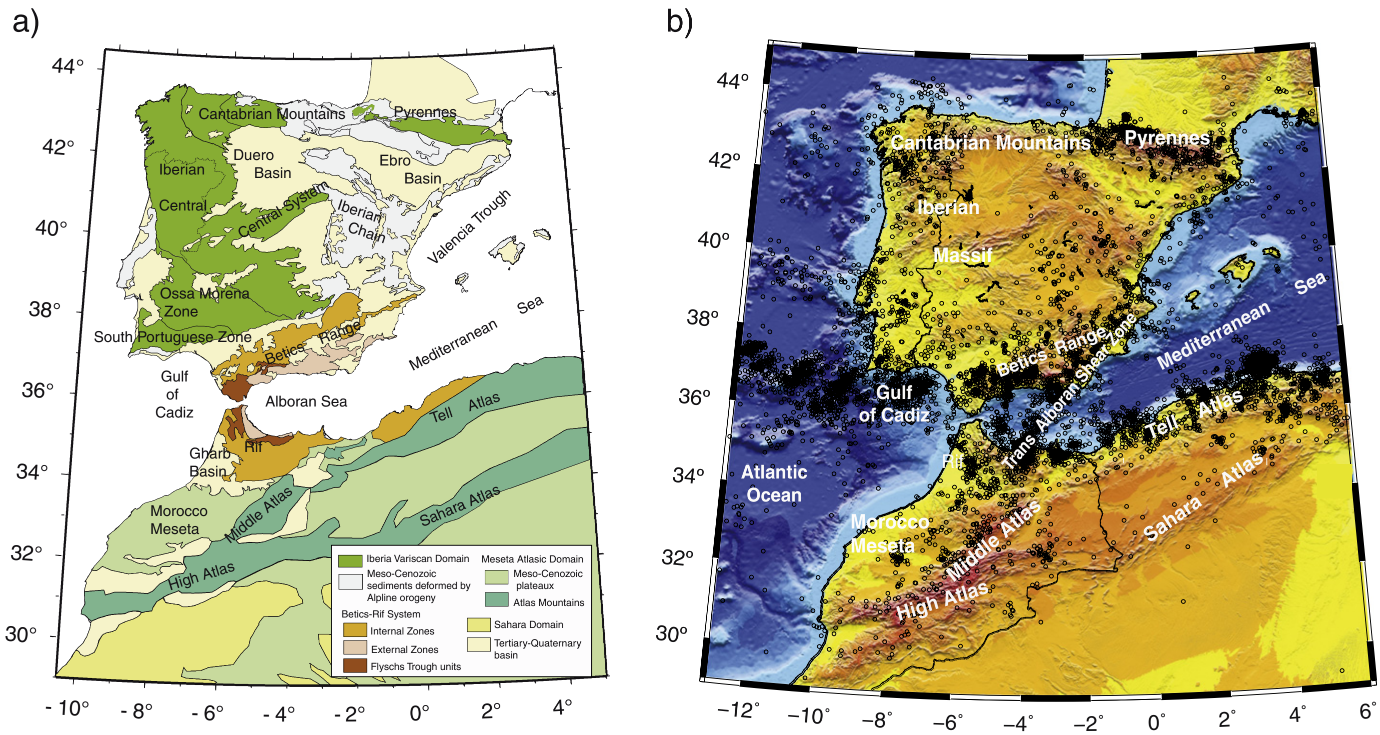

Fig. 1. a) Main geological, tectonic and geographic domains in the Iberia-Maghreb region, covering the Iberian Peninsula, NW-Africa, and nearby offshore regions (modified from Mancilla and Díaz, 2015a); b) map with the seismicity (magnitude > 3) in the Iberia-Maghreb region from ISC on-line bulletin (International Seismological Centre, www.isc.ac.uk).

The complexity of faulting patterns and seismicity distribution are a striking characteristic of regional seismotectonics, which should be properly connected to the complex geodynamic evolution of this sector of the plate boundary. Apart from oblique Nubian-Eurasian convergence, the area has been subject to extensional processes related to the Neogene evolution of the western Mediterranean (e.g., Platt and Vissers, 1989; Docherty and Banda, 1995; Comas et al., 1999; Jolivet and Faccenna, 2000). Recent analyses of GPS motion, earthquake sources and lithospheric structure suggest explaining the regional framework by a superposition of plate convergence and coeval extension (Stich et al., 2006, 2010; Koulali et al., 2011; Giaconia et al., 2012, 2013; Mancilla et al., 2012; Echeverria et al., 2013). In particular, this appears necessary to explain the differential motion of the Betic and Rif Mountains with respect to the direction of plate convergence. At least in the Betic-Rif-Alboran region, crustal deformation may be dominated by dynamic processes in the upper mantle instead of rigid plate motion (Mancilla et al., 2012). A proper analysis of earthquake source parameters is key to map the full complexity of tectonic deformation and advance in our understanding of regional geodynamics. Regional moment tensor inversion is now used systematically in the analysis of regional seismicity, providing valuable information for this purpose. In particular, two moment tensor projects on Iberia-Maghreb-scale currently provide source information with a relatively low magnitude threshold (Mw ~3.5). This includes the automated near real-time inversion by the Instituto Geográfico Nacional (IGN, Rueda and Mezcua, 2005) and the manually processed moment tensor solutions provided by the Instituto Andaluz de Geofísica (IAG, Stich et al., 2003, 2006, 2010). Despite these efforts, seismotectonic information is still scarce in several areas of low seismicity or less dense seismic broadband instrumentation, including for example the maghrebian interior. In this contribution we present a relevant update of the IAG moment tensor catalogue that overcomes some of the shortcomings and improves the record in general. A distinctive characteristic of this update is the underlying improvement of the regional seismic network during several important temporal deployments.

In the last decade, the Iberia-Maghreb region has been the target of several important research initiatives to investigate Earth's structure and dynamics. Many of these efforts are the installation of the temporary deployment of seismic instrumentation. The five years of seismicity (2009–2013) included in this study were recorded at several dense temporary deployments of seismic broadband stations in Spain and North Morocco, in addition to permanent recording networks operated by various institutions (Fig. 2). Temporary deployments are centred in the IberArray (http://iberarray.ictja.csic.es) of the TOPOIBERIA and SIBERIA projects. This broadband seismic array composed of ~80 stations was gradually covering Spain from South to North, and North Morocco since 2007, with a nominal station spacing of ~50 km (Díaz et al., 2009). This period is also covered by the INDALO project in southeastern Spain operated by IAG (López-Comino et al., 2012). From 2010, the PICASSO project (Program to Investigate Convective Alboran Sea System Overturn) deployed 85 seismic broadband stations along a roughly N–S profile from the Iberian Massif in central Spain, across the Betics and Rif Mountains, the Middle Atlas and the High Atlas and ending on the Sahara Platform, with additional stations around the Gibraltar Arc. Other projects complemented these deployments, like for example the network operated by the University of Münster with 15 broadband seismic stations deployed in the Western High Atlas. All these deployments along with the permanent broadband networks at times totalled more than 300 broadband stations operating in the Iberian-Maghreb region (Fig. 2). In particular, they provide for the first time extended regional broadband coverage in Morocco. This facilitates moment tensor analysis for small and moderate earthquake inside Morocco, and improves the coverage for northern Algerian earthquakes as well as for the surroundings of the Gibraltar Arc. The latter is clearly a key area to understand the complex and controversial geodynamic patterns under discussion. Here we show how the unprecedented station density benefits moment tensor analysis of small to moderate earthquakes (Mw 3.2–3.5) across the region, and briefly discuss the tectonic implications of the 5-year catalogue update from 2009 to 2013.

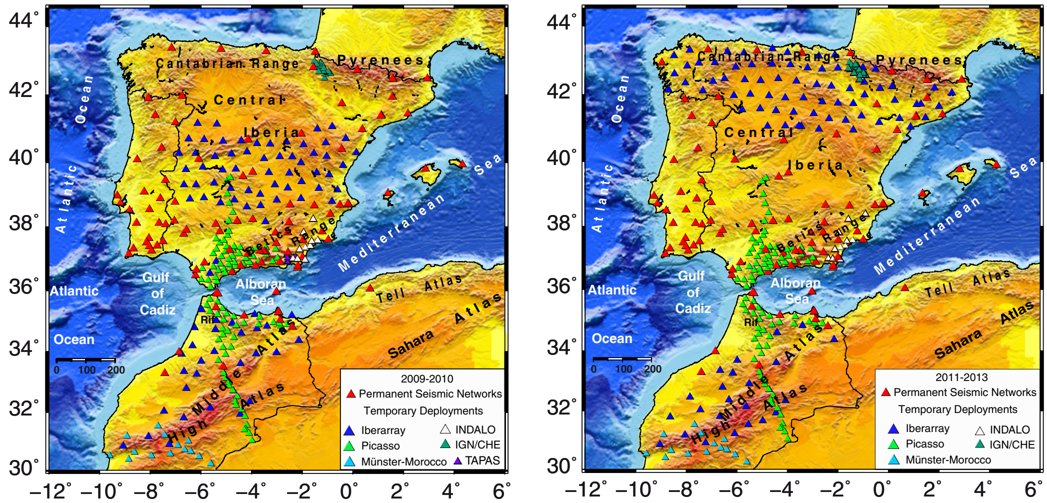

Fig. 2. Permanent and temporary broad band seismic stations recording during the second leg (2009–2010, left) and third leg (2011–2013, right) of the Iberraray deployment. Permanent broadband stations are from National Geographic Institute (IGN), Andalusian Geophysics Institute (IAG), Portuguese Sea and Atmosphere Institute, University of Lisbon, West Mediterranean network (GEOFON/ROA/UCM), Catalonian Cartographic and Geological Institute (ICGC), Observatoire de l'Ebre. Temporary broadband stations are from IberArray, Picasso, Münster-Morocco projects and IGN/CHE (Confederación hidrográfica del Ebro) partnership. Several temporary stations were not operating during the full duration of Iberraray legs, or operating during both legs.

2. Moment tensor inversion

The first order seismic moment tensor is a common and convenient representation of a seismic point source. It contains the description of the equivalent force system of a seismic event and permits to obtain the scalar seismic moment (Silver and Jordan, 1982) and the moment magnitude Mw (Hanks and Kanamori, 1979). Moment tensor inversion is a direct implementation of the representation theorem for the seismic wavefield, which establishes a linear relationship between recorded three-component waveforms, a set of Green's function derivatives or fundamental fault responses, and equivalent forces. Treating actual earthquakes with finite rupture extension, point source moment tensor inversion based on low-pass filtered waveforms yields an average orientation of force couples across the rupture surface, different from first motion focal mechanisms, which image the onset of faulting. Another relevant difference is the consideration of the complete amplitude and phase information in several different types of waves, instead of P-wave polarities alone. For tectonic earthquakes we may generally invert seismic waveforms assuming a deviatoric moment tensor and decompose the tensor into a double-couple part and a residual compensated linear vector dipole (CLVD, Jost and Herrmann, 1989). If the double couple is dominant, it can be used to infer the orientation of nodal planes (strike, dip and rake) or principal strain axes (strike and plunge), providing clues on the tectonic regime and stress axes orientations in the source region. An optional outcome from moment tensor inversion, likewise relevant for seismotectonic analyses, is an independent estimate for the depth of faulting, because the usage of body and surface waves introduces sensitivity of model misfit to the centroid depth.

Among established moment tensor projects on global, continental or regional scale (e.g., Dziewonski and Woodhouse, 1983; Pondrelli et al., 2002; Rueda and Mézcua, 2005), the largest inventory of source estimates for the Ibero-Maghreb region is currently provided by the IAG moment tensor catalogue (Stich et al., 2003). Except for a few selected events (López-Comino et al., 2012; Pedrera et al., 2012; Morales et al., 2014), IAG moment tensor solutions are published up to 2008 (Stich et al., 2010), and the purpose of this contribution is the description of a 5-year update of the catalogue, analysing seismicity from January of 2009 to December of 2013. We examine for this purpose all earthquakes with reported magnitudes ≥4 for more remote regions like Algeria or the Atlantic Ocean, ≥3.5 for the Iberian Peninsula, northern Morocco and adjacent offshore areas, and ≥3.2 for areas of particularly dense instrumentation like southern Spain. We attempt to obtain and quality check all available waveforms from permanent and operative temporary stations. Relevant filter bands to appraise waveform quality are 20s to 50s for events with Mw > 4 and 15 s to 35 s for the smallest events or where low signal-noise level is observed in the longer band. These intermediate periods filter bands are suitable for waveform inversion, following the procedure described in Stich et al., 2003. Also other aspects of the processing follow the previous practice of the IAG moment tensor catalogue to ensure the homogeneity of the moment tensor inventory, except of course the density of the available station networks, which has increased substantially during the two decades of regional seismicity, covered to date. For the computation of Green's functions we use a reflection-matrix method (Kennett, 1983; Randall, 1994), incorporating three different plane layered earth models (Stich et al., 2003) that represent the average characteristic of the lithosphere of the Iberia-Maghreb region for predominately offshore paths, for Hercynian basement and for Alpine environments, respectively. A careful manual processing is carried out, including the preprocessing and selection of waveforms, as well as a suitable weighting of waveforms along with a visual inspection of waveform matches in order to obtain a stable solution. Formal matrix inversion is carried out by minimization of the L2 norm (least squares) of the misfit between observed and predicted waveforms (Langston et al., 1982). To address the nonlinear dependence of waveform matches with source depth and obtain the best fitting combination of depth and moment tensor, we perform a grid search for focal depths with increments of 2 km in the crust and 10 km in the upper mantle. More detail on processing and inversion scheme can be found in previous descriptions of the IAG moment tensor catalogue (Stich et al., 2003, 2006).

3. Moment tensor solutions 2009–2013

In this update, we were able to obtain moment tensor solutions for 85 events (Table 1, Fig. 3). The quality of waveform matches is our principal criterion to incorporate or not an individual moment tensor estimate into the catalogue. A successful moment tensor inversion corresponds to appropriate predictions of P-waves, S-waves and surface waves at different azimuths and distances from the source. Waveform matches are assessed through visual inspection, introducing subjective criteria into the procedure, but preserving the full waveform

Table 1
IAG moment tensor solutions from the beginning of the 2009 to end of 2013. Deviatory moment tensors have been decomposed into a double-couple moment tensor and residual compensated vector dipole component (CLVD). We provide the individual elements of the deviatory moment tensor and also the strike, dip and rake of both nodal planes of the double-couple tensor (fault angles in the coordinate system of Aki and Richards, 2002), and the remained percentage of CLVD. (Note: Three new intermediate moment tensor solutions corresponding to 2014 year have been included, see text).

Date	Time	Lat	Lon	Z	Moment tensor elements [Nm]						Mo	Mw	Double couple						CLVD
[yyyymmdd]	[UTC]	[°]	[°]	[km]	mxx	mxy	myy	mxz	myz	mzz	[Nm]		Plane1 (Strike1	Dip1	Rake1)	Plane2 (Strike2	Dip2	Rake2)	[%]
20090117	11:22:26	36.38	1.58	4	−9.47e-01	4.41e−01	−2.71e−01	1.73e−01	2.23e−01	1.22e + 00	1.23e + 15	4.0	75	48	106	232	45	73	17
20090415	15:42:25	38.24	−1.16	10	−7.12e−01	−1.22e−01	6.59e−01	3.01e−02	−1.88e−01	5.27e−02	7.23e + 14	3.9	319	78	169	51	80	12	0
20090611	05:42:15	36.24	0.72	6	−3.50e−01	4.26e−01	−3.79e−01	−4.38e−01	7.84e−01	7.29e−01	1.18e + 15	4.0	56	21	112	213	70	82	5
20090705	15:50:57	36.06	−10.25	50	−2.99e + 00	3.41e−02	2.98e−02	8.31e−01	1.83e−01	2.96e + 00	3.10e + 15	4.3	93	53	94	266	37	84	1
20090818	06:56:00	35.95	−7.81	50	−1.68e−02	1.04e + 00	5.10e−01	7.58e−01	−1.71e−01	−4.93e−01	1.39e + 15	4.1	284	72	−142	180	54	−21	2
20091102	07:28:31	36.50	1.75	6	−8.60e−01	9.30e−01	−9.04e−01	−1.38e + 00	1.19e + 00	1.76e + 00	2.55e + 15	4.2	41	22	83	228	68	93	3
20091105	05:39:55	37.05	−3.82	26	9.05e−01	1.01e−01	5.77e−03	6.29e−01	5.45e−03	−9.11e−01	1.11e + 15	4.0	100	28	−83	273	62	−93	0
20091214	06:41:12	32.82	−0.09	8	3.18e + 00	4.06e + 00	−2.40e + 01	8.43e + 00	2.27e + 01	2.09e + 01	3.34e + 16	5.0	29	27	128	168	69	73	2
20091217	01:37:47	36.53	−9.78	30	−1.31e + 02	2.14e + 01	1.07e + 02	5.08e + 01	−7.79e + 01	2.43e + 01	1.54e + 17	5.4	43	83	38	307	52	171	0
20091221	02:45:04	35.20	−0.11	4	−9.58e−01	7.57e−01	−3.24e−01	1.59e + 00	−2.63e−01	1.28e + 00	2.12e + 15	4.2	75	71	104	218	24	55	2
20100121	16:57:06	34.80	−5.77	40	1.19e + 00	−5.92e + 00	−7.86e−01	1.34e + 00	1.09e + 00	−4.08e−01	6.26e + 15	4.5	274	81	−13	6	77	−170	2
20100214	22:14:30	34.79	−5.28	40	3.61e−01	−4.55e−01	6.39e−01	−6.12e−01	9.63e−01	−1.00e + 00	1.51e + 15	4.1	33	70	−92	219	21	−83	4
20100331	03:12:00	36.79	−9.80	40	−8.84e−02	−2.40e−01	1.44e−01	8.56e−01	−2.45e−01	−5.53e−02	9.31e + 14	3.9	350	17	−174	254	88	−72	1
20100401	01:36:40	43.01	0.32	18	1.13e−01	−1.69e−02	−4.03e−02	2.41e−01	1.29e−01	−7.31e−02	2.91e + 14	3.6	53	16	−152	296	83	−75	2
20100411	22:08:06	37.00	−3.69	620	2.98e + 02	−1.21e + 03	1.52e + 03	8.23e + 01	−2.78e + 03	−1.82e + 03	3.47e + 18	6.3	55	24	−44	188	73	−107	0
20100422	01:24:01	35.52	−6.64	60	−5.54e−01	3.72e−01	9.53e−02	−1.65e−01	5.99e−01	4.58e−01	8.87e + 14	3.9	96	38	148	213	71	57	10
20100514	12:29:23	35.92	4.14	2	−1.16e + 01	3.13e + 01	−4.36e + 01	−1.27e + 02	6.18e + 01	5.52e + 01	1.53e + 17	5.4	241	80	102	11	15	41	12
20100516	03:51:30	35.87	4.13	8	5.93e−02	7.55e−01	−1.68e + 00	4.57e−01	1.90e + 00	1.63e + 00	2.67e + 15	4.3	44	28	134	176	70	70	4
20100516	06:52:42	35.84	4,.05	6	−2.30e + 01	2.28e + 01	−2.80e + 01	−1.36e + 01	2.00e + 01	5.11e + 01	5.54e + 16	5.1	45	32	95	219	58	87	10
20100523	13:28:17	35.92	4.14	4	−9.18e + 01	−2.18e + 01	−1.09e + 01	−1.32e + 02	−9.20e + 01	1.03e + 02	1.89e + 17	5.5	92	18	62	301	75	98	14
20100524	21:00:42	35.95	4.15	8	6.45e−01	1.02e + 00	−1.28e + 00	−1.16e + 00	2.47e−01	6.39e−01	1.92e + 15	4.2	345	49	19	242	76	137	2
20100528	15:55:04	35.48	−2.26	14	−4.11e−01	4.31e−01	4.02e−01	−1.60e−01	−7.47e−02	9.20e−03	6.18e + 14	3.8	22	73	1	291	89	163	1
20100621	15:22:05	36.62	−6.20	40	−5.38e−02	1.36e−01	−9.27e−02	8.46e−02	6.36e−02	1.46e−01	2.15e + 14	3.5	192	53	45	70	55	133	7
20100705	10:38:11	36.57	−2.31	8	−4.46e−01	2.49e + 00	4.50e−01	1.00e−01	3.96e−01	−3.59e−03	2.56e + 15	4.2	185	87	9	95	81	177	3
20100706	14:44:05	36.69	−2.38	10	2.47e−01	1.09e + 00	−4.63e−01	2.35e−01	4.73e−01	2.16e−01	1.27e + 15	4.0	79	65	169	173	80	25	6
20100706	20:34:00	36.69	−2.37	12	7.74e−02	3.50e−01	−5.35e−02	1.52e−02	2.35e−01	−2.40e−02	4.28e + 14	3.7	354	88	−33	85	56	−177	3
20100710	19:12:33	36.55	−2.34	8	3.00e−02	1.81e−01	−4.11e−02	1.66e−02	7.29e−02	1.11e−02	1.99e + 14	3.5	84	68	176	175	86	22	2
20100710	19:18:02	36.70	−2.37	20	−2.69e−01	2.42e−01	7.25e−02	1.65e−01	1.60e−01	1.97e−01	4.12e + 14	3.7	208	53	30	98	66	139	7
20100711	09:26:03	35.76	5.34	2	−3.28e + 00	−1.00e + 00	−1.91e−01	−2.71e + 00	−1.46e + 00	3.47e + 00	4.68e + 15	4.4	98	25	76	294	66	97	2
20100711	14:15:35	35.72	5.31	6	−2.63e + 00	−7.19e−01	−9.60e−02	−5.08e + 00	−1.79e + 00	2.73e + 00	6.06e + 15	4.5	100	14	82	289	76	92	3
20100723	12:45:19	35.85	−9.86	30	−2.84e−01	4.54e−02	3.28e−01	1.91e−01	1.24e−01	−4.37e−02	3.86e + 14	3.7	218	54	−6	313	84	−144	5
20100725	20:24:41	36.28	−7.69	30	−5.04e−02	3.95e−01	9.21e−01	−8.27e−02	−9.22e−01	−8.71e−01	1.35e + 15	4.1	326	25	−113	171	67	−79	22
20100805	18:54:16	32.36	−6.08	10	−2.73e + 00	1.70e + 00	−1.01e + 00	−1.21e + 00	3.37e−01	3.73e + 00	3.95e + 15	4.4	53	36	82	243	54	96	0
20100905	03:33:47	35.20	−2.96	22	−8.41e−01	3.04e−01	8.16e−01	−1.12e−01	2.45e−01	2.51e−02	9.23e + 14	3.9	215	87	17	124	73	177	1
20100908	10:32:49	32.12	−3.72	12	−1.14e−01	−1.42e−01	5.97e−02	−4.59e−01	8.66e−02	5.41e−02	4.98e + 14	3.8	260	87	71	160	19	170	3
20101012	07:20:49	36.71	−2.58	26	−2.51e−01	2.34e−01	1.87e−01	2.87e−02	9.83e−02	6.43e−02	3.41e + 14	3.7	204	77	17	110	74	166	14
20101104	12:02:01	36.72	−2.59	12	−2.40e−01	1.12e−01	2.86e−01	1.21e−01	9.07e−02	−4.60e−02	3.26e + 14	3.6	213	61	−4	305	86	−151	22
20101104	12:02:01	36.72	−2.59	12	−1.13e + 00	4.94e−01	1.15e + 00	4.57e−01	2.04e−01	−2.16e−02	1.34e + 15	4.1	213	68	−2	304	87	−158	6
20101129	23:57:27	36.95	−12.74	50	−4.67e−01	−2.01e−01	2.92e−01	−1.73e−01	−4.10e−01	1.75e−01	6.37e + 14	3.8	66	44	16	324	79	133	8
20110214	06:04:55	32.05	−6.12	26	−6.82e + 00	1.58e + 00	6.96e + 00	−9.78e−01	4.15e−02	−1.34e−01	7.14e + 15	4.5	38	84	−4	129	85	−174	0

20110408	15:07:12	41.18	−1.08	10	−6.93e−03	1.85e−01	2.84e−01	−9.68e−02	3.28e−01	−2.77e−01	4.80e + 14	3.8	127	33	−141	3	70	−63	7
20110511	15:05:12	37.71	−1.68	6	−9.03e + 00	−1.36e + 00	2.87e + 00	1.75e + 00	4.91e + 00	6.16e + 00	9.64e + 15	4.6	127	62	129	247	46	40	3
20110511	16:47:25	37.72	−1.67	6	−6.60e + 01	−6.37e−01	2.31e + 01	1.02e + 00	2.90e + 01	4.30e + 01	6.49e + 16	5.2	121	55	135	240	54	44	7
20110511	20:37:44	37.72	−1.69	4	−6.92e−01	3.05e−01	4.19e−01	1.49e−01	2.42e−01	2.73e−01	7.33e + 14	3.9	216	63	22	115	70	151	25
20110710	22:54:21	38.34	−1.02	14	−7.71e−01	4.30e−01	6.72e−01	1.28e−01	2.63e−01	9.94e−02	8.93e + 14	3.9	118	78	163	211	74	12	0
20111013	11:15:51	38.07	0.51	6	−4.35e−01	−3.16e−01	1.70e−02	−1.54e−01	2.14e−01	4.18e−01	5.93e + 14	3.8	146	51	134	269	56	49	4
20111024	23:35:24	37.31	−1.94	16	−3.23e−01	3.08e−01	2.85e−01	−9.77e−02	−1.30e−01	3.78e−02	4.63e + 14	3.7	291	80	162	24	72	11	7
20120131	14:36:22	37.74	−3.04	16	4.39e−02	8.12e−01	1.13e−01	−1.31e−01	2.59e−01	−1.57e−01	8.73e + 14	3.9	93	71	−168	359	79	−19	12
20120218	00:28:27	34.46	−5.65	40	2.25E + 00	2.69E + 00	2.22E + 00	−5.99e−02	5.13e−01	3.48e−02	3.54E + 15	4.3	200	88	8	110	82	178	0
20120321	06:41:58	35.83	−0.64	4	5.74e−01	4.60e−01	−1.82e + 00	−2.23e + 00	2.37e + 00	1.25e + 00	3.66e + 15	4.3	220	79	108	340	21	32	2
20120324	05:50:03	36.69	0.88	12	7.97e−01	9.67e−01	−3.54e−01	−1.53e−01	7.13e−01	−4.44e−01	1.39e + 15	4.1	81	59	−158	339	71	−32	5
20120325	02:45:24	36.52	0.54	14	−5.00e−01	1.53e + 00	3.17e−01	−1.82e + 00	−8.37e−02	1.84e−01	2.42e + 15	4.2	8	41	4	275	88	131	14
20120418	09:47:25	36.48	−2.64	6	−8.96e−01	7.18e−01	2.44e + 00	1.16e + 00	−6.46e−01	−1.54e + 00	2.61e + 15	4.2	201	62	−44	316	51	−143	2
20120418	11:10:37	36.50	−2.63	6	−1.28e−01	7.47e−02	3.00e−01	1.63e−01	2.07e−02	−1.72e−01	3.17e + 14	3.6	204	53	−33	317	63	−138	1
20120425	03:18:19	36.45	1.68	18	−6.36e−01	1.71e + 01	4.73e + 00	−1.13e + 01	8.98e−01	−4.10e + 00	2.10e + 16	4.8	98	81	−146	2	56	−10	6
20120518	13:12:12	34.04	1.84	6	−1.66e−01	7.59e−01	−1.17e + 00	−2.08e−02	1.49e + 00	1.33e + 00	2.09e + 15	4.2	49	27	127	189	69	73	4
20120605	05:09:50	36.96	−10.36	40	−5.31e−01	4.72e−01	−3.38e−01	4.71e−02	−2.66e−01	8.69e−01	9.34e + 14	3.9	40	53	76	242	40	108	3
20120704	07:44:15	34.91	−2.94	12	5.11e−02	8.96e−01	−1.11e−01	5.19e−02	5.89e−01	5.96e−02	1.08e + 15	4.0	87	57	177	178	87	33	2
20120715	02:05:07	36.08	0.97	12	−3.64e−01	1.38e−01	7.19e−03	−7.94e−02	1.61e−01	3.57e−01	4.25e + 14	3.7	90	39	120	234	57	68	5
20120906	04:24:50	36.60	−2.92	10	−1.45e−01	2.17e−01	2.88e−02	−1.82e−03	1.13e−01	1.16e−01	2.78e + 14	3.6	96	57	158	198	72	35	5
20121010	06:14:40	36.46	4.50	8	−6.19e−02	−5.25e−01	−8.01e−01	−6.43e−01	−1.39e−01	8.63e−01	1.19e + 15	4.0	307	62	61	177	39	132	5
20121127	08:51:33	35.03	−2.89	6	4.93e−02	2.57e−01	9.08e−01	3.19e−01	6.30e−01	−9.57e−01	1.20e + 15	4.0	171	28	−77	338	63	−96	1
20121128	23:15:29	36.84	5.19	2	2.91e + 00	−7.89e + 00	1.50e + 01	−9.88e + 00	9.71e + 00	−1.79e + 01	2.30e + 16	4.9	38	64	−78	195	28	−111	2
20130205	21:24:13	38.02	−3.29	2	2.73e−02	2.87e−01	3.71e−02	4.48e−02	−1.65e−01	−6.44e−02	3.39e + 14	3.7	274	59	−168	177	79	−30	1
20130301	18:43:19	36.90	5.29	4	−1.86e−02	1.44e−01	4.72e−02	−1.02e + 00	−1.80e−02	−2.86e−02	1.03e + 15	4.0	360	8	−1	92	90	−98	8
20130316	09:49:23	35.83	5.60	4	−2.04e + 00	7.51e−01	3.84e + 00	−1.02e + 01	−1.00e + 01	−1.80e + 00	1.47e + 16	4.7	135	87	−102	29	12	−16	2
20130319	03:11:31	36.47	−5.48	40	−1.14e + 00	−5.78e−01	2.24e−01	2.52e−02	−6.71e−01	9.20e−01	1.37e + 15	4.1	81	49	43	320	59	130	1
20130323	02:57:39	42.82	−1.80	6	5.74e−01	1.47e−01	−5.80e−01	6.84e−02	7.08e−03	6.04e−03	5.99e + 14	3.8	142	85	5	52	85	175	1
20130404	02:27:14	37.83	−1.79	22	−2.26e−01	6.59e−01	3.01e−01	−1.89e−01	−2.39e−02	−7.54e−02	7.38e + 14	3.9	11	75	−2	101	87	−165	16
20130407	05:45:00	37.88	−1.70	22	−2.06e−02	1.15e−01	1.17e−02	−7.12e−02	−1.07e−02	8.92e−03	1.36e + 14	3.4	273	86	148	5	58	4	0
20130420	15:58:21	42.73	−1.71	4	5.26e−01	−6.17e−02	−2.73e−01	−3.29e−01	4.75e−01	−2.53e−01	7.39e + 14	3.9	47	78	−124	300	36	−20	16
20130502	18:55:35	35.60	0.08	6	1.76e + 00	3.16e + 00	−2.40e + 00	9.41e−01	2.14e + 00	6.44e−01	4.48e + 15	4.4	166	83	32	71	58	172	5
20130519	09:07:27	36.76	5.18	2	−5.46e + 00	−4.82e + 00	1.53e + 01	−8.77e + 01	−1.18e + 02	−9.83e + 00	1.47e + 17	5.4	37	5	−15	144	89	−94	9
20130526	16:00:56	36.71	5.19	4	−1.53e + 01	1.09e−01	−1.80e + 00	−2.70e + 01	3.03e + 00	1.71e + 01	3.17e + 16	5.0	93	16	98	265	75	88	12
20130613	13:24:22	38.09	−0.70	14	−8.37e−02	−1.98e−02	7.09e−02	1.92e−03	−2.93e−02	1.28e−02	8.58e + 13	3.3	320	75	163	54	74	15	2
20130621	18:40:13	36.45	−8.06	30	−4.68e−01	2.79e−01	−1.29e−01	1.23e−01	−6.77e−02	5.97e−01	6.27e + 14	3.8	61	51	90	241	39	90	9
20130704	17:25:04	37.10	−5.63	4	−2.38e−02	1.31e−02	5.55e−02	−2.36e−02	4.66e−02	−3.17e−02	7.22e + 13	3.2	136	34	−151	21	74	−59	20
20130717	03:00:56	36.55	3.02	2	−2.67e + 00	6.71e + 00	−9.22e + 00	−1.56e + 01	4.05e + 01	1.19e + 01	4.52e + 16	5.1	45	9	113	201	82	87	5
20130808	07:05:25	35.27	−4.15	4	6.24e−02	3.36e−01	2.10e + 00	4.34e−02	−3.88e−01	−2.16e + 00	2.19e + 15	4.2	348	40	−94	174	50	−86	1
20130814	19:24:13	36.33	−2.86	20	−1.98e−01	5.46e−02	1.90e−01	2.00e−02	1.11e−02	8.89e−03	2.03e + 14	3.5	217	84	0	307	90	−174	9
20131019	15:54:21	38.02	−3.26	8	−1.08e−01	9.22e−02	9.95e−02	4.57e−02	3.37e−02	8.46e−03	1.50e + 14	3.4	205	68	5	113	85	158	2
20131019	17:31:54	38.02	−3.26	8	−2.33e−02	4.54e−02	3.00e−02	1.12e−02	−2.98e−02	−6.70e−03	6.18e + 13	3.2	193	85	−30	287	59	−174	4
20131223	06:12:49	35.83	−4.30	30	−1.24e + 00	8.33e−02	1.05e−01	−2.19e−01	−5.38e−01	1.14e + 00	1.33e + 15	4.0	289	54	119	65	45	56	18
20131229	10:50:37	36.51	−2.98	4	−9.16e−02	−9.21e−02	2.39e−01	3.95e−01	−2.87e−01	−1.47e−01	5.39e + 14	3.8	342	21	−157	230	82	−69	6
20140709	18:36:23	36.88	−3.96	60	−8.72e−01	−2.31e−01	3.84e−01	−2.90e−01	−6.26e−01	4.89e−01	1.05e + 15	4.0	66	43	28	315	71	130	6.2
20140713	04:38:53	36.98	−5.52	30	4.69e−02	4.17e−02	−6.56e−02	−4.82e−02	1.40e−02	1.86e−02	8.77e + 13	3.3	239	80	144	337	54	13	0.8
20140819	13:38:24	36.96	−5.54	30	2.60e + 00	5.96e−01	−2.81e + 00	−9.43e−01	3.11e−01	2.12e−01	2.95e + 15	4.3	322	71	8	230	83	161	2.1

information including low-amplitude arrivals that are difficult to represent in a unified misfit criterion. For the large majority of events, this goal requires manual tuning of relative weighting factors, to improve the azimuthal balance and bring closer the respective contribution of different wavetypes. This step also involves downweighting or excluding problematic waveforms where indicated, such like noisy recordings (e.g., horizontal components with relevant tilt noise), near source seismograms with large amplitudes and possible near-field contribution, or waveforms that appear affected by unaccounted propagation effect in the complex lithospheric structure of the region. The final moment tensor estimate should be reasonably stable regarding moderate variations of these weighting factors. Where weighting affects the amount of CLVD component, but do not significantly change the orientation of the double couple part, we conclude that the CLVD part is not well resolved, and our policy is to release a solution with low CLVD, giving preference to a simple source model that adjusts the data. In the following, we will present and discuss briefly our catalogue update, with moment magnitudes range from 3.2 to 6.3, and centroid depths from 2 km to 620 km. The largest magnitude and depth correspond to the 11 April 2010 very deep earthquake in Southern Spain, where very deep events occur but infrequently; five such events are included in the record (Buforn et al., 2011). This seismicity has been associated to detached lithosphere from the Western Mediterranean subduction system (Faccenna et al., 2004), imaged by tomographic studies (Bezada and Humphreys, 2012; Blanco and Spakman, 1993). The moment tensor of the 2010 very deep event is straightforward to invert from regional or teleseismic body waves and will not be discussed in this contribution.

The full catalogue update presented in this work is given in Table 1, and visualized in Fig. 3 through the representation of the corresponding double couple faulting mechanisms along with the current complete IAG catalogue (Fig. 3b). New solutions consolidate established deformation patterns as well as add new facets to the overall picture. To facilitate interpretation, compressional quadrants of the mechanisms have been colour-filled according to the faulting style. Red, green and blue colours represent reverse, strike-slip and normal faulting, respectively. General orientations are represented from moment tensor eigenvectors by converting vertical components of T-, B- and P-axes into proportions of red, green and blue in the RGB colour model. We use a linear mapping of z-components (interval [0, 1]) onto 8-bit colour channels (interval [0, 255]), equivalent to combined RGB colour depth of 24 bit. Clear first order patterns of the moment tensor distributions are for example a relatively homogeneous reverse faulting regime along the entire northern margin of Algeria, consistent with NW–SE to WNW–ESE convergence (4–5 mm/yr) (DeMets et al., 1994; Calais et al., 2003; McClusky et al., 2003, Serpelloni et al., 2007; Fernandes et al., 2007) between Africa and Eurasian. Also offshore southwestern Iberia (Gulf of Cadiz and Cape St. Vincent) the deformation seems to correspond to rigid plate motion, although including more significant local heterogeneity, a larger share of strike-slip mechanisms and a larger depth extend of seismicity, reflecting the large brittle layer thickness in old oceanic lithosphere (Stich et al., 2007). In between, in the Betic-Alboran-Rif sector or Gibraltar Arc, the picture is much more complex, deformation is accommodated over a wide zone with significant seismic activity, and the deformation patterns apparently do not respond to the regional NW–SE to WNW–ESE convergence directly. Whilst in the western Betics reverse and strike-slip faulting is predominant, in the Central Betics and Southern Spain the typical solutions become normal faulting, whilst strike-slip faulting is clearly dominant in southeastern Spain. The strike-slip zone covers also most of the Alboran Sea, and is prolonged into North Morocco, where similar mechanisms are present.

At distance from this diffuse plate boundary zone, seismic deformation affects the entire Iberian Peninsula as far as the Pyrenees, and northern Africa as far as the Atlas system. Here we will look at one catalogue example each for these peripheric regions to give examples of inversion results and waveform matches. Faulting over the northern and central Iberian Peninsula is characterized mainly by normal faulting and strike-slip solutions, with a certain prevalence of strike-slip towards the west and normal faulting towards the east, including the Iberian Chain and Pyrenees, where only four Iberian intraplate mechanisms of this update are located. The new moment solution in the Iberian Chain shows normal faulting with T axes oriented NE–SW, consistent with previous solutions and active NW–SE normal faults that run along the chain, associated to the opening of Valencia Through (Simón-Gómez, 2004; Stich et al., 2003). In the Pyrenees, two new normal faulting mechanisms with NS tension axis perpendicular to the range were obtained, suggesting a scenario of postorogenic extension as previous solutions (Stich et al., 2003, 2006, 2010). For the first time, we obtain a strike-slip faulting mechanism in the Pyrenees (130323), however first motion focal mechanisms (Ruiz et al., 2005) pointed to the existence of more complex faulting patterns previously. The 2013 strike-slip solution in the western Pyrenees highlights the importance of the temporary deployments for inversion (Fig. 4) where, despite the high noise level of some recordings, acceptable waveform matches are found for Rayleigh an Love waves, as well as a low CLVD (1%) component, at reasonably low formal misfit at 6 km depth and an stable mechanism for all depths. To establish the possible context of this mechanism, we may build upon seismic profiles in the Pyrenees and Cantabrian Mountain (Pedreira et al, 2003) that have shown the presence of an E–W discontinuous delamination of the Iberian crust, with northward underthrusting along the Pyrenees-Cantabrian range. This discontinuity has been associated to the relative left-lateral displacements along NE–SW oriented structures like the Pamplona and Hendaya faults, in agreement with one of the nodal planes obtained for this event.

In the Atlas System, the situation is fundamentally different insofar as this sector was not covered by the moment tensor catalogue previously. Temporary networks were crucial to obtain several source estimates in this update. We show the example of a reverse faulting mechanism obtained in the Sahara Atlas, in Algeria, close to the Algerian-Moroccan border. This mechanism (091214) shows almost WNW–ESE P axis orientation and appears similar to another mechanism further northeast (120518) that will be discussed below. We present the result and data matches of the moment tensor inversion of the first mechanism in Fig. 5. Similar solutions for this event are provided by the INGV Euro-Mediterranean moment tensor catalogue and the global CMT catalogue, however a strike-slip solution was obtained by ETHZ (www.emsc-csem.org). The quality of waveform matches obtained with our solution for records in Morocco and South Iberia, as well as the low CLVD (1%) component of the moment tensor, suggest that the reverse mechanism may be the most appropriate solution for this event. We will analyse the patterns observed along the Atlas System in a dedicated subsection below, as well as other moment tensor solutions according to their geographical affinity. This includes northern Algeria, the Betic-Alboran shear zone and the SW Iberian margin, where the catalogue update consolidates the deformation patterns observed previously, as well as the already mentioned

Fig. 3. a) New moment tensor solutions for the 5-year period 2009–2013. The double couple tensor is plotted in lower hemisphere projection. Moment tensors are labelled with the year, month and day of the event and, where is necessary, a capital letter (A–D) is indexed for events occurred in the same day according to the temporal order of events (Table 1). Compresional quadrants are colour-filled using a linear mapping of vertical components of eigenvectors to the RGB colour model (see RGB colour triangle for association of red, green and blue components to reverse, strike-slip and normal faulting earthquakes, respectively). b) Full IAG moment tensor catalogue; representation like Fig. 3a).

a)

b)

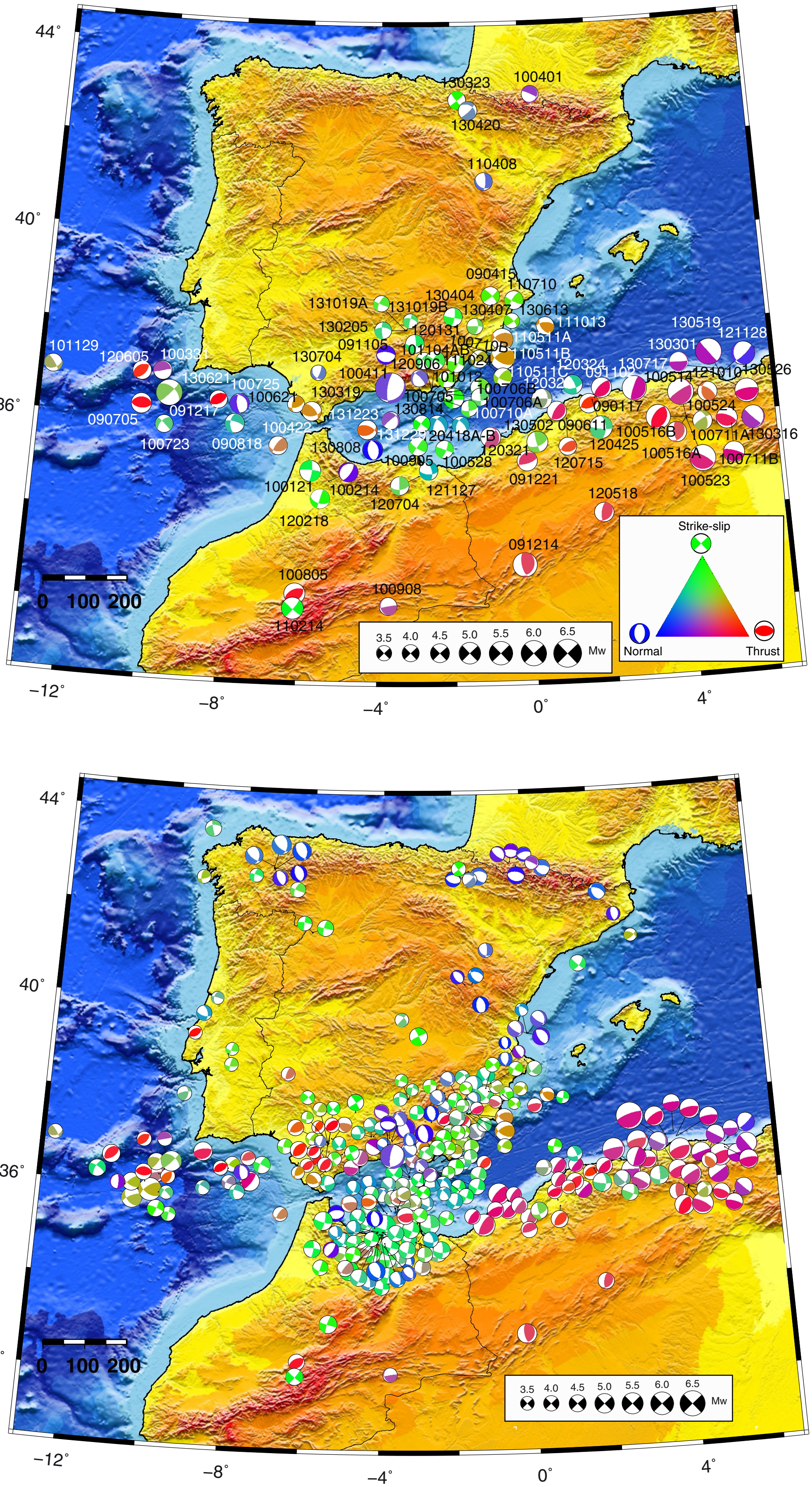
44°
40°
36°
32°
−12°
−8°
−4°
0°
4°
0 100 200
130323
100401
130420
110408
090415
110710
130404
131019A
131019B
130407
130613
111013
130205
120131
110511A
130519
121128
091105
110511B
130301
130704
120906
120324
130717
100411
101012
100514
121010
130526
101129
120605
100331
130621
100725
100621
130319
100705
100706B
100706A
090117
100524
090705
091217
130814
100710A
130502
090611
100516B
100711A
130316
100723
090818
100422
131223
120418A-B
120425
100516A
100711B
130808
100905
100528
120321
120715
100121
100214
121127
091221
100523
120704
120518
120218
091214
100805
100908
110214
3.5
4.0
4.5
5.0
5.5
6.0
6.5
Mw
Strike-slip
Normal
Thrust

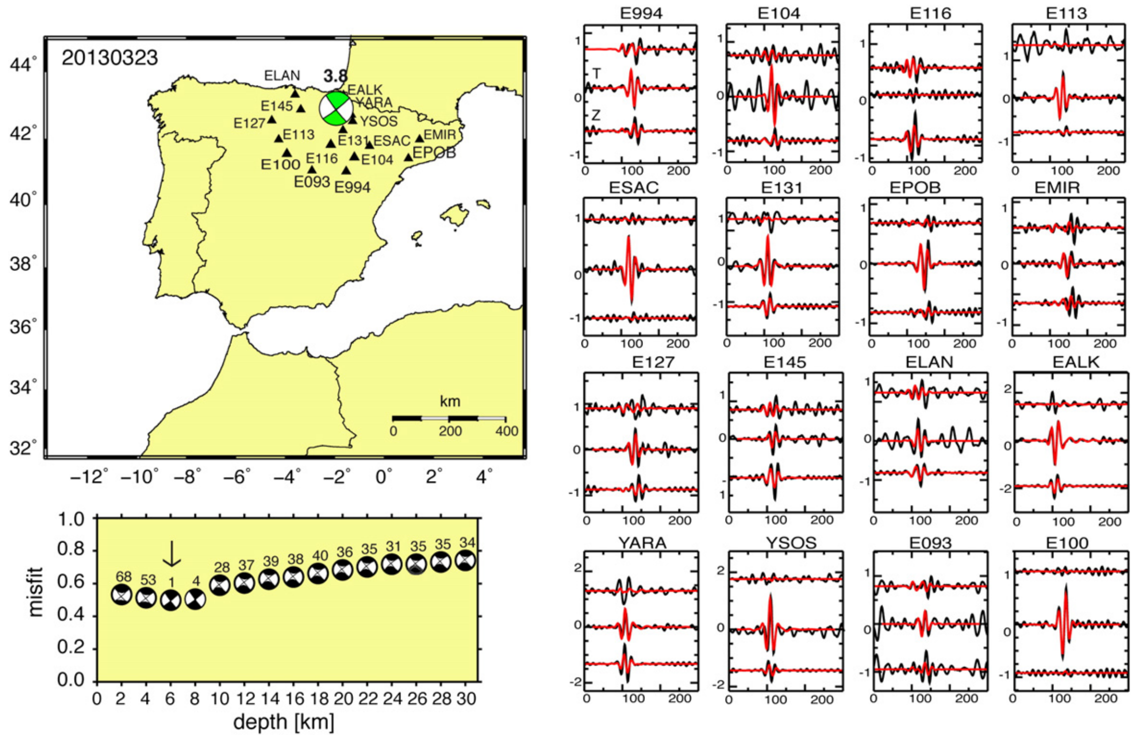

Fig. 4. Moment tensor inversion result for the Mw 3.8, 23 April 2013, Pyrennes earthquake. The map shows the location of stations and the best solution in equal-area, lower hemisphere projection. Below, we show the inversion result for different trial depths, indicating minimum misfit and minimum CLVD component (small numbers above mechanisms) at 6 km depth. Waveform matches at 16 near-regional stations display observed seismograms in grey and moment tensor predictions in black. In each station panel, the radial, transverse and vertical components of displacement are plotted from top to bottom (displacement in 10^{-6} m and time in seconds).

Atlas System and the surroundings of the Gibraltar Arc, where new solutions significantly enhance the sampling of lithospheric deformation. Another key region, the Betic range, is not well represented in this update, except for a normal faulting mechanism (091105) at the Granada basin compatible with NNE–SSW extension pattern and previous solutions (Galindo-Zaldívar, 1999; Stich et al., 2003) and four strike-slip mechanisms near the Central Betic mountain front in the Eastern Guadalquivir Basin (130121, 130205, 1310191a, 131019b) (Morales et al., 2014).

3.1. Northern Algeria

Northern Algeria presents the most intense seismicity in the Ibero-Maghreb region, mainly occurring at shallow depth in a narrow belt running along the coastline. Also in this catalogue update, solutions for Algeria form the largest geographical subset. Previous mechanisms show pure reverse and strike-slip faulting (Stich et al., 2006, 2010). These solutions are in agreement with GPS observations and show that a significant part of the Nubia-Eurasia plate convergence is accommodated at the Algerian margin by N30°W oriented shortening (Stich et al., 2006, Serpelloni et al., 2007). We present 25 moment tensor solutions along the Mediterranean margin of Algeria with magnitudes ranging from Mw 3.7 to 5.4 with source depth from 2 to 8 km. The solutions near the coastline show the same compressional pattern faulting as previous solutions, i.e., inverse faulting solutions with a systematic counterclockwise rotation of P axes orientations from E to W, mixed and some strike-slip faulting solutions. Two clusters of events have been obtained further inland. The first, with three events (100711A-B, 130316), show similar faulting solutions as previous solutions at those longitudes, with NE–SW P axis orientations. The second, with five solutions (100514, 100516A-B, 100523, 100524) present a more complex faulting pattern, showing reverse faulting with nearly orthogonal kinematics probably reflecting local stress and fault interaction in the source region.

3.2. Betic-Alboran Shear Zone

The Betic-Alboran Shear-Zone (De Larouzière et al., 1988) is a NE–SW trending belt of left-lateral faults extending from Alicante (East Iberia) into Almeria (Southeast Iberia) and further on across the Alboran Sea to the Mediterranean Moroccan margin. Previous moment tensor solutions for the shear zone (Stich et al., 2005b, 2006) show predominantly strike-slip faulting with minor normal or reverse component and some normal mechanisms. Also in this update, faulting solutions for the Betic–Alboran shear zone show the expected dominance of strike-slip faulting. Several of the mechanisms occur along or in the vicinity of major faults in the Betic-Alboran Shear-Zone. We were able to include 12 new solutions (100705, 100706A-C, 100710A-B, 101104A-B, 111024, 120906, 130404) for the Carboneras fault sector (e.g., Gràcia et al., 2006; Rutter et al., 2012). This area at the SE tip of Spain was poorly represented in the previous catalogue. New mechanisms are all similar, showing nearly strike-slip faulting style with NNE–SSW oriented left-lateral and WNW–ESE oriented right-lateral nodal planes. The former planes correspond to the general trend of the Betic–Alboran shear zone, whilst the latter may be interpreted as conjugate faulting. Generally we do not discriminate between fault and auxiliary plane in point source moment tensor inversion, however some events appear to be associated to conjugate faults, given their spatial proximity to mayor structures (e.g., 101104A-B, Pedrera et al., 2012). Formal estimates of centroid depth for these earthquakes range from 6 to 26 km, meaning that some of these events would be located below the Moho depth of ~19 km, according to P-wave receiver functions (Mancilla et al., 2015a,b). The corresponding depth estimates, however, are poorly constrained according to the low variability of L2 misfit with source depth. The low sensitivity to focal depth may reflect a reduced azimuthal coverage for some events and a predominance of Love waves in the inversion, in addition to a possible systematic bias due to strong lateral variations of lithospheric structure at the margin.

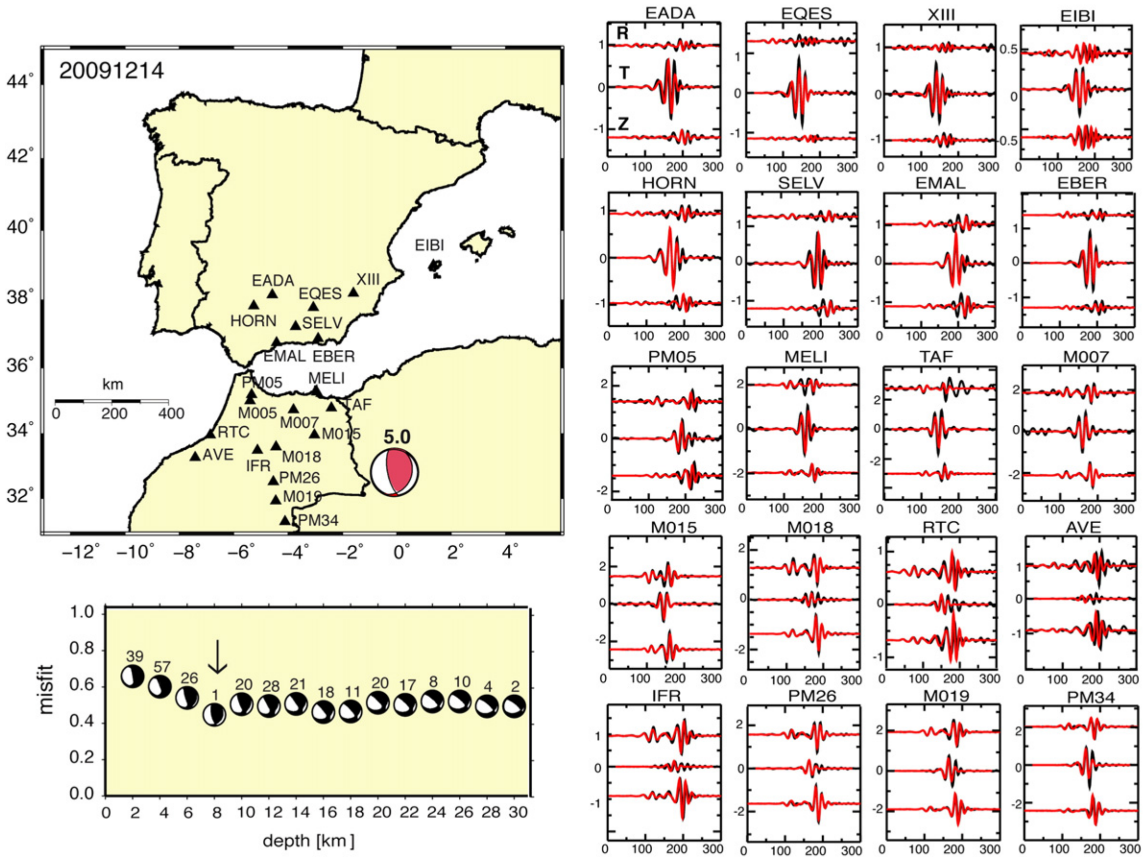

Fig. 5. Moment tensor inversion result for the Mw 5.0, 14 December 2009, Sahara Atlas (Algeria) earthquake. The map shows the location of stations and the best solution in equal-area, lower hemisphere projection along the inversion result. Adequate waveform matches are found (observed waveforms in black and predictions in red), for seismic stations in Morocco and Iberian Peninsula. Radial, transverse and vertical components of displacement are plotted from top to bottom versus time in seconds (displacements in 10^{-5} m and time in seconds).

In this sector, three normal faulting mechanisms (120418A-B, 131229) have also been obtained, with nodal plane striking in agreement with mapped normal faults in this area (Martínez-Díaz and Hernández-Enrile, 2004). Three oblique reverse solutions (110511A-C) can be associated to a major structure named Alhama de Murcia Fault (Martínez-Díaz, 2002; Masana et al., 2004), which hosted a destructive earthquake near the city of Lorca in 2011 (López-Comino et al., 2012). These mechanisms show NW dipping nodal planes coincident with the local strike and the kinematics of the fault, previously recognized as being active and having oblique reverse kinematics. These mechanisms, as well as two new strike-slip solutions in the western of this fault, are equally consistent with the regional strike-slip deformation pattern, given a good coincidence between the N–S directions of moment tensor P-axes (N167°E–N190°E) and N–S maximum horizontal shear stress in SE-Spain [Stich et al., 2006, 2010; de Vicente et al., 2008]. Three new solutions (090415, 110710, 130613) in the northern limit of the Betic shear zone show strike-slip moment tensors with nodal planes in agreement with fault orientations within the Betic-Alboran shear zone. Near the southern termination of the shear zone at the Morocco margin, we obtained three strike-slip earthquakes (100905, 121127, 120704), similar to previous solutions near the Nekor fault (Stich et al., 2005b). An event at the central Morocco margin shows a normal faulting mechanism with E–W tension axis orientation compatible with the strike-slip and extensional stress regime pattern in this region.

3.3. Offshore Southwestern Iberia

This region forms the transition between a simple linear Eurasian-Nubian plate boundary in the Atlantic Ocean from the Azores to approximately the Gorringe Bank (11.5° W) and the distributed deformation observed on the Gibraltar arc on either side of the Straits of Gibraltar (5° W). Dominant structures are several WNW–ENE trending bathymetric lineaments (Bartolomé et al., 2012), forming a band of deformation know as the SWIM fault zone (Zitellini et al., 2009). Perpendicular to these lineaments, there are several active NE–SW trending west verging folds and thrusts (e.g., Gràcia et al., 2003). Previous moment tensors solutions show predominantly WNW–ESE right-lateral strike-slip motion oblique to the direction of plate convergence and reverse mechanisms in agreement with the mapped fault network (Stich et al., 2005b, 2010). Seismicity in this sector is characterized by a depth extend from shallow till upper mantle depths (8–60 km). Subcrustal seismicity with similar deformation patterns as the shallow events indicate crust–mantle coupling in the old, oceanic lithosphere with large brittle layer thickness (Sallarès et al., 2011, Stich et al., 2005a, 2007). In this update, we present four solutions in the Gulf of Cadiz (090818, 100422, 100725, 130521) with depths ranging from 30 km to 60 km and magnitude Mw from 3.5 to 4.1. These solutions present reverse and strike-slip faulting with NW–SE trending P axis and a normal mechanism with similar T axis orientation. Several solutions were obtained in Cape St. Vincent (090705, 091217, 100331, 120605) at upper mantle depths. They present strike-slip to reverse mechanisms according to previous solutions and regional faulting pattern and NS to NW–SE P- axes orientations. This group includes the largest event of the catalogue update in this sector with moment magnitude Mw 5.4, at 30 km depth (091217).

3.4. The Atlas System

The Atlas System is an intracontinental mountain belt limited by thrust faults. It was formed during the alpine cycle in North Africa within a regional scale compressional framework. The Atlas is trending nearly linear SW–NE except for its central part, which is divided into two branches: the Middle-Atlas, which follows a SSW–NNE direction, and the High Atlas trending aproximately E–W. The High Atlas connects with the Sahara Atlas in Algeria. GPS studies indicate that deformation along the Middle and High Atlas is still active, suggesting that this belt is presently accommodating up to 1 mm yr^{-1} WNW–ESE oriented shortening (Fadil et al., 2006, Serpelloni et al., 2007). However, seismicity in the Atlas System is scarce and diffuse with magnitudes usually smaller than 5, except for the 29 February 1960 Agadir earthquake ($M = 5.7$) and two events in the easternmost Anti-Atlas ($M = 5.5$). These earthquakes show shallow hypocentres and dominantly strike-slip or reverse mechanisms (Medina and Cherkaoui, 1991; El Alami et al., 1992; Medina, 2008). Events with magnitudes between 4 and 5 Mw occur concentrated in a narrow, NNE–SSW trending zone at the junction between Middle-Atlas and the High Atlas. This alignment is parallel to the NNW–SSE Imilchil transverse fault. The regional seismicity distribution is coincident with the location of a NE–SW trending uplift of the asthenosphere (e.g., Missenard et al., 2006). Recent studies support that the High Atlas is not compensated isostatically, showing only moderate shortening and crustal thickening, and propose that the elevations are conduced by thermal domains (Zeyen et al., 2005; Teixell et al., 2005; Ayarza et al., 2005; Missenard et al., 2006; Fullea et al., 2010). Given the typically low magnitudes of seismicity and the remote location with respect to permanent seismic networks in the Ibero-Maghreb region, no moment tensor solutions for this area have been present in the IAG moment tensor catalogue so far. In this update, the deployment of temporary instrumentation in Morocco allows for addressing five earthquakes that occurred in the period 2009–2013 (example in Fig. 5). Among them, we discuss one reverse solution in the Southern Middle Altas and one strike-slip mechanism in the Central High Atlas. These solutions apparently reproduce the main seismotectonic trends in this region: the reverse mechanism shows nodal planes with NE–SW striking and NW–SE P-axis orientation in agreement with the plate convergence direction (Serpelloni et al., 2007); the strike-slip solutions presents a NE–SW trending nodal plane similar to previous solutions obtained by focal mechanisms studies (Medina and Cherkaoui, 1991; Medina, 2008). Another solution further east shows a reverse faulting mechanism with similar trend of principal axes. We also obtained two new solutions in the Sahara Atlas, in Algeria. The two reverse mechanisms show almost WNW–ESE P-axes orientations. Whilst only five solutions along such a long mountain belt still do not provide a satisfactory sampling of seismotectonic deformation, all these new solutions show nodal planes following the trend of the belt and P-axes orientation according to the Iberia and Nubia plate convergence. These homogeneous characteristics suggest that reverse faulting mechanisms in the Atlas system reflect the accommodation of Nubia-Eurasia plate convergence through ongoing active shortening in the mountain belt, coincident with available evidence from GPS observations (Serpelloni et al., 2007).

3.5. Gibraltar Arc

The Betic-Rif orogen constitutes an arcuate fold and trust belt formed by the interaction of Nubia-Eurasia plate convergence and relative westward motion of Alboran domain. Both branches of the orogeny compose the Gibraltar arc. Heterogenous faulting patterns are present in this arc, and in particular in its northern, Betic branch, where more data are available (Stich et al., 2003, 2006, 2010). In particular, extension observed in the central Betics does not agree with predicted NNW–SSE Iberia-Nubia plate convergence, indicating more complex tectonic processes. Recent GPS studies show W and SW displacements of the western Betics and Rif, respectively, requiring active extension in the area (Stich et al., 2006; Koulali et al., 2011). The coverage with available moment tensor mechanism has been fairly dense at the legs of the arc, especially the northern branch, but sparse near the vertex of the structure around the Strait of Gibraltar. In this update, new moment tensor solutions (Fig. 6) were obtained in the surrounding of the Gibraltar Arc. An interesting characteristic of these solutions is source depth; most of them locate below 25 km depth in the lower crust or uppermost mantle. These deeper events with small magnitudes are complicate to address in full waveform moment tensor inversion because of the low surface wave radiation; we were able to include them mainly thanks to the improvement of station coverage.

Previous moment tensors from subcrustal earthquakes at the arc can be classified into two groups. One group corresponds to intermediate deep events at a curved lineament of seismicity near ~4.5° W with N–S trend, dipping southward from crustal depths beneath the Betics to a depth of ~120–150 km beneath the centre of the Alboran Sea (e.g., Buforn et al., 1991, 1997; Morales et al., 1997). There is a tendency of these solutions to show one subvertical and one subhorizontal nodal plane, but their azimuthal orientations are variable. This update contributes one offshore solution for this lineament (131223) with ~ N–S P-axis in the western Alboran Sea, however this solution is located at significantly shallower depth (30 km) than other subcrustal earthquakes in this sector. Two further solutions were obtained for the connection of this lineament to the deep crustal levels of the central Betics (140709 at 60 km depth and 091105 at 30 km depth). The former shows faulting style similar to other intermediate deep mechanisms in this sector, whilst the latter corresponds to normal faulting mechanisms with ~N–S T-axis, more similar to shallow earthquakes in the central Betics. The second well established concentration of subcrustal seismicity occurs in the Gulf of Cadiz, connecting to subcrustal earthquakes at Cape St. Vincent. Three new mechanisms are contributed by this update (090818, 100725, 130621), showing reverse, normal and strike-slip faulting respectively. Reverse and strike-slip solutions are consistent with previous solutions indicating transpression at the plate boundary. Here we report two more reverse faulting solutions with NW–SE compressional axes further east (100422, 100621), at 60 km and 40 km depth, respectively, that appear to extend this deformation pattern towards the Strait of Gibraltar.

Analysing the faulting solutions below 25 km below the Gibraltar arc, between these established groups, we find a striking heterogeneity and a very disperse geographical distribution, covering the entire extension of the belt between the Betic and Rif mountain fronts. This includes a slightly oblique reverse faulting solution (130319) located at 40 km depth, showing NE–SW P-axes orientation. This is almost perpendicular to reverse faulting solutions for the Gulf of Cadiz, and can be assumed as being unrelated to plate convergence. A normal faulting mechanism with SE–NW T-axis orientation at 40 km depth has been obtained in the Southernwestern Rif (100214). The rest of faulting solutions below 25 km at the Gibraltar arc correspond to strike-slip faulting, however showing significantly heterogeneous orientations. On the Iberian side, we find two strike-slip events below the NW-Betic mountain front (140713, 140819). Shallow earthquakes in this sector show active NW–SE shortening (Ruiz-Constán et al., 2009). In northern Morocco, a new strike-slip solution at 40 km depth with NW–SE P-axis orientation according to plate convergence has been obtained beneath the Gharb basin (120218). Remarkably, this solution is close to the previously mentioned normal faulting mechanism showing NW–SE extension, as well as close to another strike-slip solution with nearly opposite kinematics (100121).

The different characteristics of deep crustal and subcrustal earthquakes in the Gulf of Cadiz, Gibraltar arc and Alboran region correlate with structural heterogeneity in tomographic images (Fig. 6, Villaseñor et al., 2007; Bezada et al., 2013; Palomeras et al., 2014; Chertova et al., 2014; Bonnin et al., 2014; Villaseñor et al., 2015). In the Gulf of Cadiz, upper mantle earthquakes occur in old, authochtonous oceanic lithosphere and nearby continental domains, and can be related to crust mantle coupling at the SW-Iberian margin (Stich et al., 2007). At the Gibraltar arc, lower crustal and subcrustal earthquakes correlate with a pronounced low velocity anomaly that leaves a very clear

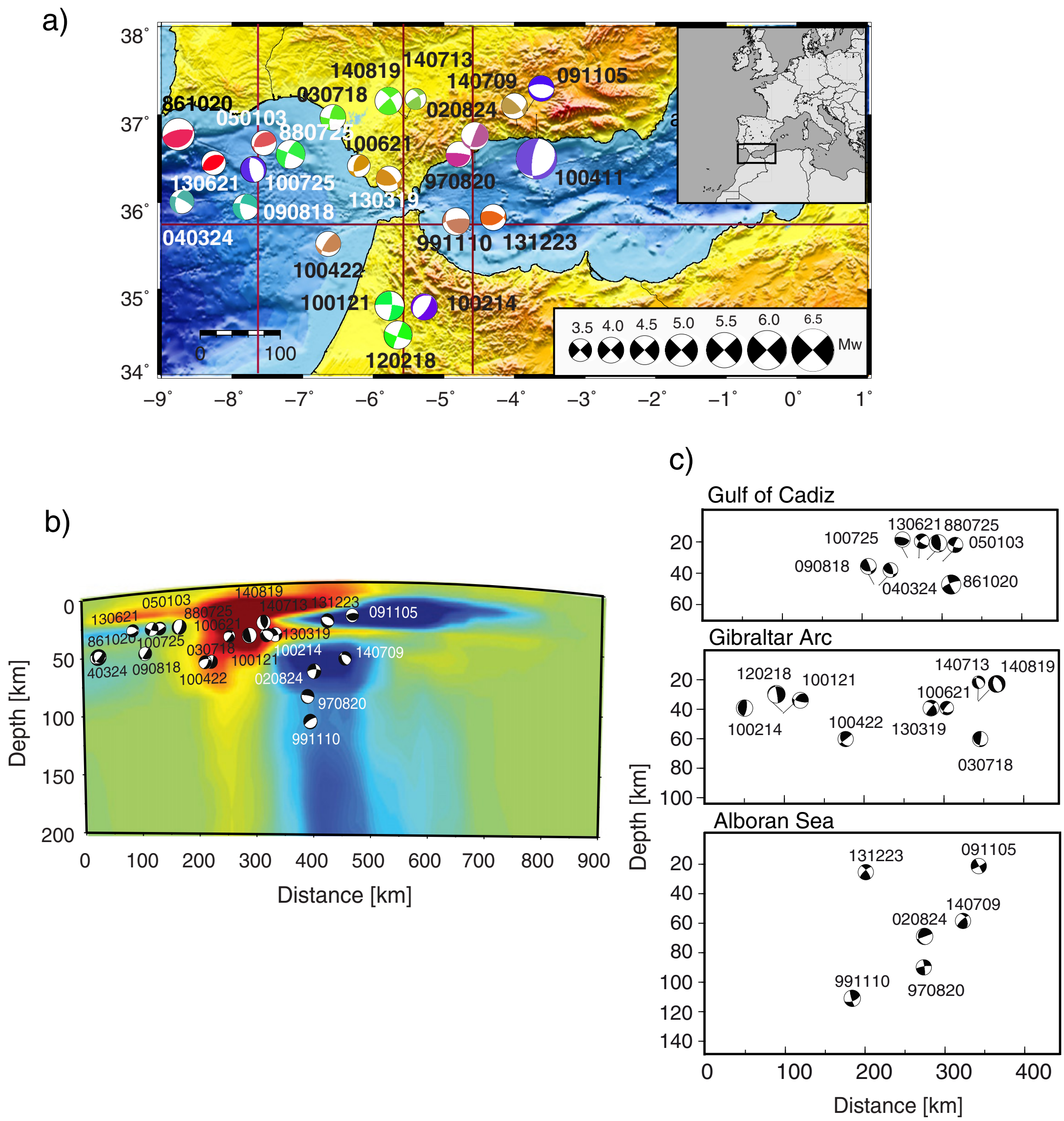

Fig. 6. a). Moment tensor solutions with depth > 25 km in the surroundings of the Gibraltar arc (Betic-Rif orogen, Alboran Sea and Gulf of Cadiz) available in the IAG catalogue. We included several moment tensor solutions for intermediate depth earthquakes in 2014 to complete the picture (140709, 140713, 140819). Beach ball colours represent the faulting style (see Fig. 3). b) W–E vertical cross section near the Strait of Gibraltar (red line in upper map) showing the superposition of P-wave velocity structure (from Bezada et al., 2013) and the projection of mechanisms for intermediate depth earthquakes into a S–N line of sight. C) N–S Vertical cross sections for intermediate depth earthquakes associated to the delaminating slab, the low velocity region below the arc, and the transitional and oceanic lithosphere, respectively.

signature also in phase velocities deduced from noise crosscorrelations (Silveira et al., 2013). The complex faulting pattern emerging from these mechanisms is not easy to interpret in terms of geodynamics. In particular, there are examples of nearby solutions with kinematics that would practically cancel each other, like strike slip solutions with opposite sense of shear beneath the Rif mountain front. The variability of moment tensor mechanisms includes both faulting style and axes orientations. Further east, deep crustal and subcrustal earthquakes are associated to a high velocity anomaly in the upper mantle. However, these solutions appear unrelated to active subduction, where moment tensor principal axes should align with the dip of the downgoing lithosphere (Isacks and Molner, 1971). Similar dip values, but variable horizontal orientations for intermediate events beneath the Alboran Sea suggest a possible dominance of vertical forces in the process, indication for a possible delamination scenario driven by buoyancy. From recent studies of deep lithospheric structure (Mancilla et al., 2012, 2013, 2015b,c), we may associate this intermediate seismicity with downgoing continental lithosphere in this sector. These structural elements appear to reflect delaminating slabs in the western Betics and South Rif, indicating that deformation in the Iberian-Maghreb plate boundary is conditioned by active subcrustal processes, apart from plate convergence. The heterogeneous faulting pattern for deeper earthquakes appears to reflect the complex interplay of both agents, and a geodynamic model where oceanic subduction has developed into continental delamination in western Betics and Rif.

4. Conclusions

We present 84 recent moment tensor solutions adding to the IAG moment tensor catalogue, improving the seismotectonic picture of the Iberia-Maghreb region in several ways. The majority of solutions consolidate the previously recognized patterns of moment tensors in the region (Stich et al., 2003, 2006, 2010). This holds for example for the Mediterranean margin of Algeria, the SW Iberian margin, the Betic range and the Trans-Alboran shear zone. In northern Algeria, new reverse and strike-slip solutions confirm active compression. Offshore the SW Iberia margin, new strike-slip and reverse solutions behave according to the transpressive character of the Eurasian-Nubia plate boundary and confirm that this deformation style affects both the crust and the brittle uppermost oceanic mantle down to ~60 km depth. In the Betic-Rif region, we refine the details of the progression of faulting styles from mainly shear faulting in the east to extension in central part and transpressive deformation in the west, incorporating new strike-slip solutions at the central part of the mountain front. The left-lateral Trans-Alboran Shear Zone, connecting eastern Spain with the Moroccan margin, is sampled significantly better with the present update, including new, consistent solutions over the entire extension of the shear zone, and most relevantly along the Carboneas fault sector. Within established deformation regimes, an intrinsic tendency of catalogue updates appears to be the increase of heterogeneity, reflecting that an improved sampling is more probable to cover the full range of natural parameter variability. This happens for example in the Pyrennes, where a new and well-contrained strike-slip mechanism breaks the previous hegemony of normal faulting mechanisms. Altogether, the high quality permanent seismic network along with the dense temporary deployments during 2009–2013 provided an enhanced regional waveforms database for our analysis, permitting to reduce the magnitude threshold of moment tensor solutions in several areas and favouring the inclusion of events that may be conditioned by local stresses.

The most significant update of the catalogue probably corresponds to the Atlas System and to intermediate deep earthquakes in the Betic-Rif-Alboran region. New solution for the Atlas System, an area where no solutions were available previously in the IAG catalogue, display how reverse and strike-slip mechanisms accommodate the plate convergence by shortening in the belt. New moment tensor solution of small to moderate earthquakes (Mw 3.2–3.5) in the immediate vicinity of the Gibraltar Arc reflect how the favourable recording conditions with a large density of seismic stations allow for reducing the magnitude threshold. The most curious solutions obtained in Betic-Rif-Alboran region are earthquakes at lower crustal or subcrustal depth (>25 km), where heterogeneous faulting styles are obtained from normal to reverse mechanisms, including opposite kinematics in some cases. This heterogeneity appears to indicate the superposition of different geodynamic processes, in particular extensional processes coeval to oblique plate convergence compression. Extension may be driven by delamination as inferred from recent studies of P-receiver functions (Mancilla et al., 2013., 2015c).

The catalogue update was marked by an important densification of the underlying broadband seismic networks, an important part of which corresponded to temporary installations. Evidently, a better coverage with seismic broadband stations increases the possibility to have enough suitable waveforms to obtain well-constrained moment tensor solutions, especially in structurally heterogeneous environments where complex wave propagation affects our ability to fit the recordings. However, it is not clear beforehand how temporary deployments may add to a moment tensor project in a region of low to moderate seismicity, which is a long term effort compared to the duration of seismic experiments. Temporary instrumentation cannot substitute high quality permanent networks in such initiatives, however they may permit to obtain valuable individual samples of deformation where the deployments coincide with suitable earthquakes. In intraplate Iberia and the Pyrenees, the areas where the main improvement of broadband coverage is obtained with the second and third leg of the IberArray deployment, only four new mechanisms were obtained. This fact reflects the relatively low seismic activity in these areas in general, and during this 5-year update in particular. Large parts of western intraplate Iberia, for example, did not produce any usable events for this update, whilst the catalogue coverage from previous seismicity is fair. However, the IberArray deployment was highly useful to improve azimuthal coverage for many events in the Betic-Alboran region and at the SW Iberian margin. The situation is different with the INDALO deployment in southeastern Spain which was crucial for local earthquakes in the Betic-Alboran shear zone and Betic range in this update; in particular it was important to densify the moment tensor inventory available for the Carboneras sector of the Betic-Alboran shear zone. The same holds for the temporary deployments of the IberArray, Picasso, and Münster-Morocco projects in Morocco. These stations were pivotal for obtaining moment tensor estimates in the Atlas system and stabilizing inversions at the Gibraltar Arc, the two areas that show the most important improvements. The heterogeneous and complex faulting patterns over the Iberia-Maghreb region as well as the persisting lack of solution in several areas calls for further enhancements of the regional moment tensor inventory for a better understanding of regional geodynamics. Temporary deployments may be a highly valuable complement for such efforts.

Acknowledgments

We are grateful to Jose Miguel Azañon and José Antonio Álvarez Gómez for detailed and constructive comments on the original version of this manuscript. We also want to express our gratitude to those responsible of permanent networks (IAG, IGN, MedNet/INGV, IRIS, Orfeus, Geofon/ROA/UCM, ICGC-Barcelona, Observatori de l'Ebre, IST-Lisbon, IM/FCUL-Portugal) as well as all personnel working in the Topoiberia, INDALO, Picasso and Münster-Morocco temporary networks for acquiring and sharing high quality seismic broadband data. This is a contribution of the Consolider-Ingenio 2010 project TOPO-IBERIA [CSD2006-00041]. Additional funding was provided by projects CGL2008-01830 and CGL2012-31472. We used free software GMT (Wessel and Smith, 1998) and SAC (Goldstein et al., 2003).

References

Aki, K., Richards, P.G., 2002. Quantitative Seismology. 2nd edition. University Science Books, New York.

Ayarza, P., Alvarez-Lobato, F., Teixell, A., Arboleya, M.L., Teson, E., Julivert, M., Charroud, M., 2005. Crustal structure under the central High Atlas Mountains (Morocco) from geological and gravity data. Tectonophysics 400, 67–84.

Bartolomé, R., Gràcia, E., Stich, D., Martínez–Loriente, S., Klaeschen, D., Masana, E., Diez, S., Lo Iacono, C., Moreno, X., Zitellini, N., Mànuel, A., Dañobeitia, J.J., 2009. Evidence for active strike-slip faulting along the Eurasia-Africa convergence zone: implications for seismic hazard in the southwest Iberian margin. Geology 40 (no. 6), 495–498. http://dx.doi.org/10.1130/G33107.1 (June 2012).

Bartolomé, R., Gràcia, E., Stich, D., Martínez–Loriente, S., Klaeschen, D., Masana, E., Diez, S., Lo Iacono, C., Moreno, X., Zitellini, N., Mànuel, A., Dañobeitia, J.J., 2012. Evidence for active strike-slip faulting along the Eurasia-Africa convergence zone: Implications for seismic hazard in the southwest Iberian margin. Geology 40 (6), 495–498. http://dx.doi.org/10.1130/G33107.1 (June).

Bezada, M.J., Humphreys, E.D., 2012. Contrasting rupture processes during the April 11, 2010 deep-focus earthquake beneath Granada, Spain. Earth Planet. Sci. Lett. 353–354, 38–46.

Bezada, M.J., Hymphreys, E.D., Toomey, D.R., Harnafi, M., Dávila, J.M., Gallart, J., 2013. Evidence for slab rollback in westernmost Mediterranean from improved upper mantle imaging. Earth Planet. Sci. Lett. 368.

Blanco, M.J., Spakman, W., 1993. The P-wave velocity structure of the mantle below the Iberian Peninsula: evidence for subducted lithosphere below southern Spain. Tectonophysics 221, 13–34.

Bonnin, M., Nolet, G., Villaseñor, A., Gallart, J., Thomas, C., 2014. Multiple-frequency tomography of the upper mantle beneath the African/Iberian collision zone. Geophys. J. Int. 198, 1458–1473.

Buforn, E., Udias, A., Madariaga, R., 1991. Intermediate and deep earthquakes in Spain. Pure Appl. Geophys. 136, 375–393. http://dx.doi.org/10.1007/BF00878576.

Buforn, E., Sanz de Galdeano, Carlos, Udías, A., 1995. Seismotectonics of the Ibero-Maghrebian region. Tectonophysics 248 (3-4), 247–261. http://dx.doi.org/10.1016/0040-1951(94)00276-F.

Buforn, E., Coca, P., Udías, A., Lasa, C., 1997. Source mechanism of intermediate and deep earthquakes in southern Spain. J. Seismol. 1, 113–130. http://dx.doi.org/10.1023/A:1009754219459.

Buforn, E., Bezzeghoud, M., Udías, A., Pro, C., 2004. Seismic sources on the Iberia–African plate boundary and their tectonic implications. Pure Appl. Geophys. 161, 623–646.

Buforn, E., Pro, C., Cesca, S., Udías, A., del Fresno, C., 2011. The 2010 Granada, Spain, deep earthquake. Bull. Seismol. Soc. Am. 101, 2418–2430.

Calais, E., DeMets, C., Nocquet, J.M., 2003. Evidence for a post-3.16-Ma change in Nubia-Eurasia-North America plate motions? Earth Planet. Sci. Lett. 216, 8–92.
Chertova, M.V., Spakman, W., Geenen, T., van den Berg, A.P., van Hinsbergen, D.J.J., 2014. Underpinning tectonic reconstructions of the western Mediterranean region with dynamic slab evolution from 3-D numerical modeling. J. Geophys. Res. Solid Earth 119, 5876–5902. http://dx.doi.org/10.1002/ 2014JB011150.
Comas, M.C., Platt, J.P., Soto, J.I., Watts, A.B., 1999. The origin and tectonic history of the Alboran Basin: insights from leg 161 results. In: Zahn, R., Comas, M.C., Klaus, A. (Eds.), *Proc. ODP, Sci. Res.*, vol. 161, Ocean Drilling Program, College Station TX, pp. 555–580.
De Larouzière, F., de Bolze, J., Bordet, P., Hernandez, J., Montenat, C., Ott d'Estevou, P., 1988. The Betic segment of the lithospheric Trans Alboran shear zone during the Late Miocene. Tectonophysics 152, 41–52.
De Vicente, G., Cloetingh, S., Muñoz-Martín, A., Olaiz, A., Stich, D., Vegas, R., Galindo-Zaldívar, J., Fernández-Lozano, J., 2008. Inversion of moment tensor focal mechanisms for active stresses around the Microcontinent Iberia: tectonic implications. Tectonics 27. http://dx.doi.org/10.1029/2006TC002093.
DeMets, C., Gordon, R.G., Argus, D.F., Stein, S., 1994. Effect of recent revisions to the geomagnetic reversal time scale on estimates of current plate motions. Geophys. Res. Lett. 21, 2191–2194.
Díaz, J., Villaseñor, A., Gallart, J., Morales, J., Pazos, A., Córdoba, D., Pulgar, J., García-Lobón, J.L., Harnafi, M., Group, TopoIberia Seismic Working, 2009. The IberArray broadband seismic network: a new tool to investigate the deep structure beneath Iberia. Orfeus Newsl. 8 (2).
Docherty, C., Banda, E., 1995. Evidence for the eastward migration of the Alboran Sea based on regional subsidence analysis: a case for basin formation by delamination of the subcrustal lithosphere? Tectonics 14, 804–818.
Dziewonski, A.M., Woodhouse, J.H., 1983. An experiment in the systematic study ofglobal seismicity: centroid moment-tensor solutions for 201 moderate and largee arthquakes of 1981. J. Geophys. Res. 88, 3247–3271.
Echeverria, A., Khazaradze, G., Asensio, A., Gárate, J., Martin Davila, J., Surinach, E., 2013. Crustal deformation in eastern Betics from CuaTeNeo GPS network. Tectonophysics 608, 600–612. http://dx.doi.org/10.1016/j.tecto.2013.08.020.
El Alami, S.O., Medina, F., Jebli, H., 1992. Etude du séisme d'Agadir du 5 avril 1992. Gaia, Lisboa 5, 1–5.
Faccenna, C., Piromallo, C., Crespo-Blanc, A., Jolivet, L., Rossetti, F., 2004. Lateral slab deformation and the origin of the western Mediterranean arcs. Tectonics 23, TC1012. http://dx.doi.org/10.1029/2002TC001488.
Fadil, A., Vernant, P., McClusky, S., Reilinger, R., Gomez, F., Ben Sari, D., Mourabit, T., Feigl, K., Barazangi, M., 2006. Active tectonics of the western Mediterranean: evidence for roll-back of a delaminated subcontinental lithospheric slab beneath the Rif Mountains Morocco. Geology 34, 529–532.
Fernandes, R.M.S., Miranda, J.M., Meijninger, R.M.L., Bos, M.S., Noomen, R., Bastos, L., Ambrosius, B.A.C., Riva, R.E.M., 2007. Surface velocity field of the Ibero-Maghrebian segment of the Eurasia–Nubia plate boundary. Geophys. J. Int. 169, 315–324.
Fullea, J., Fernàndez, M., Afonso, J.C., Vergés, J., Zeyen, H., 2010. The structure and evolution of the lithosphere–asthenosphere boundary beneath the Atlantic–Mediterranean Transition Region. Lithos 120 (1–2), 74–95. http://dx.doi.org/10.1016/j.lithos.2010.03.003.
Galindo-Zaldívar, J., Jabaloy, A., Serrano, I., Morales, J., González-Lodeiro, F., Torcal, F., 1999. Recent and present-day stresses in the Granada Basin (Betic Cordilleras): example of a late Miocene present-day extensional basin in a convergent plate boundary. Tectonics 18, 686–702.
Giaconia, F., Booth-Rea, G., Martínez-Martínez, J.M., Azañón, J.M., Pérez-Peña, V., Pérez-Romero, J., Villegas, I., 2012. Geomorphic evidence of active tectonics in the Sierra Alhamilla (eastern Betics, SE Spain). Geomorphology 145–146 http://dx.doi.org/10.1016/j.geomorph.2011.12.043 (90–106).
Giaconia, F., Booth-Rea, G., Martínez-Martínez, J.M., Azañón, J.M., Pérez-Romero, J., Giménez, J., Suriñach, Villegas, I., 2013. Mountain front migration and drainage captures related to fault segment linkage and growth: the Polopos transpressive fault zone (southeastern Betics, SE Spain). J. Struct. Geol. 46 (0), 76–91. http://dx.doi.org/10.1016/j.jsg. 2012.10.005.
Goldstein, P., Dodge, D., Firpo, M., Lee, Minner, 2003. SAC2000: signal processing and analysis tools for seismologists and engineers. In: Lee, W.H.K., Kanamori, H., Jennings, P.C., Kisslinger, C. (Eds.), IASPEI International Handbook of Earthquake and Engineering Seismology. Academic Press, London.
Gràcia, E., Danobeitia, J., Verges, J., Bartolome, R., 2003. Crustal architecture and tectonic evolution of the Gulf of Cadiz, SW Iberia, at the convergence of the Eurasian and African plates. Tectonics 22 (4), 1033. http://dx.doi.org/10.1029/2001TC901045.
Gràcia, E., et al., 2006. Active faulting offshore SE Spain (Alboran Sea): implications for earthquake hazard assessment in the Southern Iberian Margin. Earth Planet. Sci. Lett. 241, 734–749.
Hanks, T.C., Kanamori, H., 1979. A moment magnitude scale. J. Geophys. Res. 84, 2348–2350.
Isacks, B., Molnar, P., 1971. Distribution of stresses in the descending lithosphere from a global survey of focal-mechanism solutions of mantle earthquakes. Rev. Geophys. Space Phys. 9, 103–174. http://dx.doi.org/10.1029/RG009i001p00103.
Jolivet, L., Faccenna, C., 2000. Mediterranean extension and the Africa–Eurasia collision. Tectonics 19 (6). http://dx.doi.org/10.1029/2000TC900018 1095-1106.
Jost, M.L., Herrmann, R.B., 1989. A student's guide and review to moment tensors. Seismol. Res. Lett. 60, 37–57.
Kennett, B.L.N., 1983. Seismic Wave Propagation in Stratified Media. Cambridge Univ. Press, New York.
Koulali, A., Ouazar, D., Tahayt, A., King, R.W., Vernant, P., Reilinger, R.E., McClusky, S., Mourabit, T., Davila, J.M., Amraoui, N., 2011. New GPS constraints on active deformation along the Africa-Iberia plate boundary. Earth Planet. Sci. Lett. v. 308, 211–217.
Langston, C.A., Barker, J.S., Pavlin, G.B., 1982. Point-source inversion techniques. Phys. Earth Planet. Inter. 30, 228–241.
López-Comino, J.A., Mancilla, F., Morales, J., Stich, D., 2012. Rupture directivity of the 2011, Mw 5.2 Lorca earthquake (Spain). Geophys. Res. Lett. 39. http://dx.doi.org/10.1029/2011GL050498.
Mancilla, F., Stich, D., Morales, J., Julià, J., Diaz, J., Pazos, A., Córdoba, D., Pulgar, J.A., Ibarra, P., Harnafi, M., Gonzalez-Lodeiro, F., 2012. Crustal thickness variations in northern Morocco. J. Geophys. Res. 117. http://dx.doi.org/10.1029/2011JB008608.
Mancilla, F., Stich, D., Berrocoso, M., Martín, R., Morales, J., Fernandez-Ros, A., Páez, R., Pérez-Peña, A., 2013. Delamination in the Betic Range: deep structure, seismicity, and GPS motion. Geology 41, 307–310.
Mancilla, F., Díaz, J., 2015a. High resolution Moho topography map beneath Iberia and Northern Morocco from Receiver Functions analysis. Tectonophysics 663, 205–213.
Mancilla, F., Stich, D., Morales, J., Martín, R., Diaz, J., Pazos, A., Córdoba, D., Pulgar, J.A., Ibarra, P., Harnafi, M., Gonzalez-Lodeiro, F., 2015b. Crustal Thickness and Images of the Lithospheric discontinuities in the Gibraltar arc and surrounding areas. Geophys. J. Int. (accepted).
Mancilla, F., Booth-Rea, G., Stich, D., Pérez-Peña, J.V., Morales, J., Azañón, J.M., Martín, R., Giaconia, F., 2015c. Slab rupture and delamination under the Betics and Rif constrained from receiver functions. Tectonophysics 663, 214–226.
Martínez-Díaz, J.J., 2002. Stress field variations related to fault interaction in a reverse oblique-slip fault: the Alhama de Murcia fault, Betic Cordillera, Spain. Tectonophysics 356, 291–305.
Martínez-Díaz, J.J., Hernández-Enrile, J.L., 2004. Neotectonics and morphotectonics of the Southern Almeria (Betic-Cordillera-Spain) kinematics implications. Int. J. Earth Sci. 93, 189–206.
Masana, E., Martínez-Díaz, J.J., Hernández-Enrile, J.L., Santanach, P., 2004. The Alhama de Murcia fault (SE Spain), a seismogenic fault in a diffuse plate boundary: seismotectonic implications for the Ibero-Magrebian region. J. Geophys. Res. 109, B01301. http://dx.doi.org/10.1029/2002JB002359.
McClusky, S., Reilinger, R., Mahmoud, S., Ben Sari, D., Tealeb, A., 2003. GPS constraints on Africa (Nubia) and Arabia plate motions. Geophys. J. Int. 155, 126–138.
Medina, F, 2008. Catalogue of focal mechanisms of the Moroccan earthquakes for the period 1959–2007. Doc. Inst. Sci. 23, 58 (Rabat).
Medina, F., Cherkaoui, T.E., 1991. Focal mechanisms of the Atlas earthquakes, and their tectonic implications. Geol. Rundsch. 80, 639–648.
Missenard, Y., Zeyen, H., Frizon de Lamotte, D., Leturmy, P., Petit, C., Sébrier, M., Saddiqi, O., 2006. Crustal versus asthenospheric origin of the relief of the Atlas mountains of Morocco. J. Geophys. Res. 111, B03401. http://dx.doi.org/10.1029/2005JB003708.
Morales, J., Serrano, I., Vidal, F., Torcal, F., 1997. The depth of the earthquake activity in the Central Betic (southern Spain). Geophys. Res. Lett. 24, 3289–3292.
Morales, J., Azañón, J.M., Stich, D., Roldán, F.J., Pérez-Peña, J.V., Martín, R., Cantavella, J.V., Martín, J.B., Mancilla, F., González-Ramón, F.A., 2014. The 2012–2013 earthquake swarm in the eastern Guadalquivir basin (South Spain): a case of heterogeneous faulting due to oroclinal bending. Gondwana Res. http://dx.doi.org/10.1016/j.gr.2014.10.017.
Palomeras, I., Thurner, S., Levander, A., Liu, K., Villasenor, A., Carbonell, R., Harnafi, M., 2014. Finite-frequency Rayleigh wave tomography of the western Mediterranean: mapping its lithospheric structure. Geochem. Geophys. Geosyst. 15, 140–160. http://dx.doi.org/10.1002/2013GC004861.
Pedreira, D., Pulgar, J.A., Gallart, J., Díaz, J., 2003. Seismic evidence of Alpine crustal thickening and wedging from the western Pyrenees to the Cantabrian Mountains (north Iberia). J. Geophys. Res. 108 (B4), 2204. http://dx.doi.org/10.1029/2001JB001667.
Pedrera, A., Galindo Zaldívar, J., Marín Lechado, C., García Tortosa, F.J., Ruano, P., López Garrido, A.C., Azañón, J.M., Peláez, J.A., Giaconia, F., 2012. Recent and active faults and folds in the central-eastern Internal Zones of the Betic Cordillera. J. Iber. Geol. 38, 191–208.
Platt, J.P., Vissers, R.L.M., 1989. Extensional collapse of thickened continental lithosphere: A working hypothesis for the Alboran Sea Gibraltar Arc. Geology 17, 540–543.
Pondrelli, S., Morelli, A., Ekström, G., Mazza, S., Boschi, E., Dziewonski, A.M., 2002. European–Mediterranean regional centroid-moment tensors: 1997–2000. Phys. Earth Planet. Inter. 130, 71–101.
Randall, G.E., 1994. Efficient calculation of complete differential seismograms for laterally homogeneous earth models. Geophys. J. Int. 118, 245–254.
Rueda, J., Mezcua, J., 2005. Near-real-time seismic moment-tensor determination in Spain. Seismol. Res. Lett. 76, 455–465.
Ruiz, M., Gallart, J., Díaz, J., Olivera, C., Pedreira, D., López, C., González-Cortina, J.M., Pulgar, J.A., 2005. Seismic activity at the Western Pyrenean edge. Tectonophysics 412, 217–235.
Ruiz-Constán, A., Stich, D., Galindo-Zaldívar, J., Morales, J., 2009. Is the northwestern Betic Cordillera mountain front active in the context of the convergent Eurasia–Africa plate boundary? Terra Nova 21, 352–359. http://dx.doi.org/10.1111/j.1365-3121.2009.00886.x.
Rutter, E.H., Faulkner, D.R., Burgess, R., 2012. Structure and geological history of the Carboneras Fault Zone, SE Spain: part of a stretching transform fault system. J. Struct. Geol. 45, 68–86.
Sallarès, V., et al., 2011. Seismic evidence for the presence of Jurassic oceanic crust in the central Gulf of Cadiz (SW Iberian margin). Earth Planet. Sci. Lett. http://dx.doi.org/10.1016/j.epsl.2011.09.003.
Silveira, G., Dias, N.A., Villaseñor, A., 2013. Seismic imaging of the Western Iberian Crust using ambient noise: boundaries and internal structure of the Iberian Massif. Tectonophysics 589, 186–194. http://dx.doi.org/10.1016/j.tecto.2012.12.025.

Serpelloni, E., Vannucci, G., Pondrelli, S., Argnani, A., Casula, G., Anzidei, M., Baldi, P., Gasperini, P., 2007. Kinematics of the Western Africa–Eurasia plate boundary from focal mechanisms and GPS data. Geophys. J. Int. 169, 1180–1200.

Silver, P.G., Jordan, T.H., 1982. Optimal estimation of scalar seismic moment. Geophys. J. R. Astron. Soc. 70, 755–787.

Simón-Gómez, J.L., 2004. La estructura extensional neógena-cuaternaria en la Cordillera Ibérica. In: Vera, J.A. (Ed.), Geología de España. Sociedad Geológica de España-IGME, Madrid. ISBN: 84-7840-546-1, pp. 615–617.

Stich, D., Ammon, C.J., Morales, J., 2003. Moment tensor solutions for small and moderate earthquakes in the Ibero-Maghreb region. J. Geophys. Res. 108, 2148. http://dx.doi.org/10.1029/2002JB002057.

Stich, D., Mancilla, F., Morales, J., 2005a. Crust-mantle coupling in the Gulf of Cadiz (SWIberia). Geophys. Res. Lett. 32. http://dx.doi.org/10.1029/2005GL023098.

Stich, D., Mancilla, F., Baumont, D., Morales, J., 2005b. Source analysis of the Mw 6.3 2004 Al Hoceima earthquake (Morocco) using regional apparent source time unctions. J. Geophys. Res. 110. http://dx.doi.org/10.1029/2004JB003366.

Stich, D., Serpelloni, E., Mancilla, F., Morales, J., 2006. Kinematics of the Iberia-Maghreb plate contact from seismic moment tensors and GPS observations. Tectonophysics 426, 295–317.

Stich, D., Mancilla, F., Pondrelli, S., Morales, J., 2007. Source analysis of the February 12th 2007, Mw 6.0 Horseshoe earthquake: implications for the 1755 Lisbon earthquake. Geophys. Res. Lett. 34. http://dx.doi.org/10.1029/2007GL030012.

Stich, D., Martín, R., Morales, J., 2010. Moment tensor inversion for Iberia-Maghreb earthquakes 2005–2008. Tectonophysics 483 (3), 390–398.

Teixell, A., Ayarza, P., Zeyen, H., Fernandez, M., Arboleya, M.L., 2005. Effects of mantle upwelling in a compressional setting: the Atlas Mountains of Morocco. Terra Nova 17, 456–461.

Villaseñor, A., Yang, Y., Ritzwoller, M.H., Gallart, J., 2007. Ambient noise surface wave tomography of the Iberian Peninsula: implications for shallow seismic structure. Geophys. Res. Lett. 34. http://dx.doi.org/10.1029/2007GL030164.

Villaseñor, A., Chevrot, s, Harnafi, M., Gallart, J., Pazos, A., Serrano, I., Córdoba, D., Pulgar, J.A., Ibarra, I., 2015. Subduction and volcanism in the Iberia-North Africa collision zone from tomographic images of the upper mantle. Tectonophysics 663, 240–251.

Wessel, P., Smith, W.H.F., 1998. New, improved version of the Generic Mapping Tools released. Eos. Trans. AGU 79, 579.

Zeyen, H., Ayarza, P., Fernàndez, M., Rimi, A., 2005. Lithospheric structure under the western African-European plate boundary: a transect across the Atlas Mountains and the Gulf of Cadiz. Tectonics 24, TC2001. http://dx.doi.org/10.1029/2004TC001639.

Zitellini, N., Gràcia, E., Matias, L., Terrinha, P., Abreu, M.A., DeAlteriis, G., Henriet, J.P., Dañobeitia, J.J., Masson, D.G., Mulder, T., Ramella, R., Somoza, L., Diez, S., 2009. The quest for the Africa-Eurasia plate boundary west of the Strait of Gibraltar. Earth Planet. Sci. Lett. 280 (1-4), 13–15.